ABSTRACT

SULLIVAN, ROBERT JOSEPH. Investigation of Hyperfine Interaction, Spin Polarization, Spin Delocalization, and Structure-Property Relationships of Organic Based Exchange-Coupled Biradicals. (Under the direction of Dr. David A. Shultz).

The focus of the Shultz research group is to explore the magnetic properties of radical systems and to gain insight to the process by which unpaired electrons communicate. An additional objective is to gain an understanding of exchange-coupled systems at the molecular level in order to elicit controllable and predictable responses to perturbations of these systems. We accomplish these goals with molecular structure-property relationships derived from several molecular series possessing correlated, unpaired electrons. Structure-property relationships of exchange-coupled systems is a relatively unexplored frontier in chemistry. It is within this frontier that our work is of paramount importance.

An emerging field of molecular electronics research takes advantage not only of the electron's charge, but also its spin -- so called "spintronics." [1] In the following document, I will present three projects, the results of which might help fashion future components of molecular spintronic devices. In addition, these projects represent the first magnetostructural correlations of their kind, and as such require little justification. The descriptions of these projects are as follows:

1) Controlling ferromagnetic exchange: Substituent effects on the singlet-triplet gap in bis-semiquinone (SQ) biradicals.
2) Bond torsion dependence and the development of an empirical H_{AB} scale in exchange- coupled Donor-Bridge-Acceptor (DBA) type biradicals
3) Inhibition of back electron transfer/light-induced excited state spin trapping (LIESST) effect in DBA biradicals bound to a redox-active iron (III).

The information obtained from these projects is useful to the advancement of spintronic technologies and can be used to enhance our knowledge of electron transfer and molecular magnetic properties.

The purpose of the following document is threefold. First, it presents the background of the field of molecular magnetism. Second, the previous accomplishments of the Shultz research group will be introduced. Finally, the aforementioned projects will be explored in depth, including established initiatives for future work.

The future work includes multistep syntheses, as well as numerous characterization experiments that must be conducted. Considerable progress has been made concerning both the substituent effects project and Donor-Bridge-Acceptor project. Progress will continue to be made over the next few years. The LIESST effect project, the most recent and arguably most interesting, has seen little development due to its infancy. My primary focus over the next three years will center on developing the LIESST effect and torsion dependence projects.

Investigation of Hyperfine Interaction, Spin Polarization, Spin Delocalization, and Structure-Property Relationships of Organic Based Exchange-Coupled Biradicals

by
Robert Joseph Sullivan

A dissertation submitted to the Graduate Faculty of
North Carolina State University
in partial fulfillment of the
requirements for the degree of
Master of Science

Chemistry

Raleigh, North Carolina

2015

APPROVED BY

David A. Shultz Committee Chair	Christopher B. Gorman

Walter Weare

BIOGRAPHY

Ubie Sullivan was born to Jill and Lt. Col. Michael J. Sullivan USAF Ret. In Clovis, New Mexico. Growing up in a military family afforded Ubie the unique opportunity to live and visit places all over the world.

Ubie excelled on the wrestling team throughout middle school and high school, which culminated with a freestyle state championship title in his weight class. When time allows, he continues to help out with wrestling teams in the area.

Throughout his young life, Ubie was always exceedingly curious about the way things worked and how they were put together. Known as a the child that asked a million questions, Ubie discovered a love for a field of study with a million unanswered questions: the field of Chemistry. That love is what drew Ubie to pursue a degree in Chemistry at North Carolina State University.

He married the love of his life, Tasha, in 2007 on the beach in Costa Rica. They welcomed to the world their first son, Tobren Cole Sullivan "Tobie" in 2013.

Ubie graduated from NC State in 2006 with a BA in chemistry and a minor in Chemical Engineering. In his spare time, Ubie loves to employ his engineering skills by building wood projects around the house.

ACKNOWLEDGEMENTS

This work would not have been possible without the tremendous support and assistance I received from many individuals in my life. I am forever grateful for the emotional support from family members, knowledge from fellow scientists, and guidance from friends. I would be remiss if I did not take this time to thank the people who have truly made this work possible.

The gratitude I have for my advisor Dr. Dave Shultz is beyond measure. Over the years, Dave has become not only a mentor, but also a friend. Dave's intelligence is awe-inspiring, yet he remains humble. He is a man I look up to and someone I emulate. The five years I spent working with Dave were some of the most rewarding, interesting, and fun times of my entire life. My relationship with Dave is a great treasure.

In addition, I need to thank my wife, Tasha Sullivan, for the unbelievable amount of support she has given me over the years. Words cannot describe the relationship I have with Tasha. Without her my life would have no meaning. She supports me when I need support, challenges me when I need to be challenged, is a friend when I need a friend, and possesses the wisdom to know which roll I need most at the time. She means the world to me and is without doubt the most important person in my life. In addition I would like to thank my son Tobie for making my life complete. I love you.

I also need to thank my family: My Mom, Jill; my father, Michael; and Brother, Obie. Throughout my entire life, in times of trouble and times of joy, my Mother has always been there for me. She has always been there to pick me up when I fall and encourage me in all my endeavors. My brother has always been a source of inspiration to me, the confidence he has in me has nurtured a confidence in myself.

I would like to thank Geoff Lewis "Bitzer" for always having the courage to stick to his guns and force me to think about science in different lights. His friendship has really shaped the scientist I have become.

I also need to thank Professors Chris Gorman, Walter Weare, and Elon Ison for all the valuable scientific discussions and guidance.

TABLE OF CONTENTS

LIST OF TABLES

LIST OF FIGURES

Chapter I

Introduction, Background, and Theory

1.1 Introduction:

"I have worked in the field of molecular magnetism for almost two decades and I have been more and more fascinated by the beauty of this area and by the diversity it presents."[2]

--Olivier Kahn

The force of magnetism is a phenomenon that has fascinated scientists in all fields of study since the beginning of human discovery and inquest. From the initial discovery of magnetite to the incorporation of qubits in quantum computers, magnetism has played an integral role in society.[3] Though ancient in its discovery, the science surrounding magnetism still holds overwhelming potential for research and ground-breaking applications.

Magnetism as a physical property can be divided into two main categories: paramagnetism and diamagnetism (Figure I.1). Paramagnetism arises from unpaired electrons and is manifest as an attraction to an externally applied magnetic field. Diamagnetism arises from core- and valence paired electrons and presents itself as repulsion to an external magnetic field. Every substance in nature displays diamagnetism to some degree: if it has paired electrons it has diamagnetism. Within these two main categories, several sub-categories of magnetism exist as well (Figure I.1).

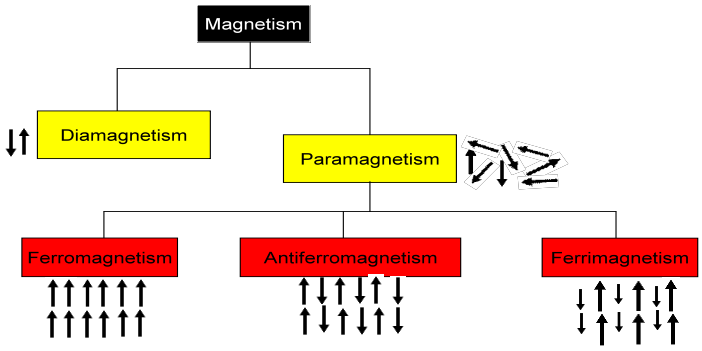

Figure I.1. Bulk magnetic properties found in 3 dimensional materials

As shown in Figure I.1, three primary sub-categories involving bulk magnetic properties are listed under the paramagnetism heading: ferro-, antiferro-, and ferrimagnetism.[4] The above classifications are a representation of bulk properties possessed by different materials. In the Shultz research group, we study the molecular analogs to these bulk properties. Rather than focus on ferromagnetism, we focus on ferromagnetic coupling. Similarly, we study antiferromagnetic coupling rather than antiferromagnetism (Figure I.2). Ferromagnetic materials possess a permanent magnetic moment in the absence of an external field and manifest large and permanent magnetizations. These substances are attracted to an external field, rather than being repelled, as is the case of diamagnetic materials.

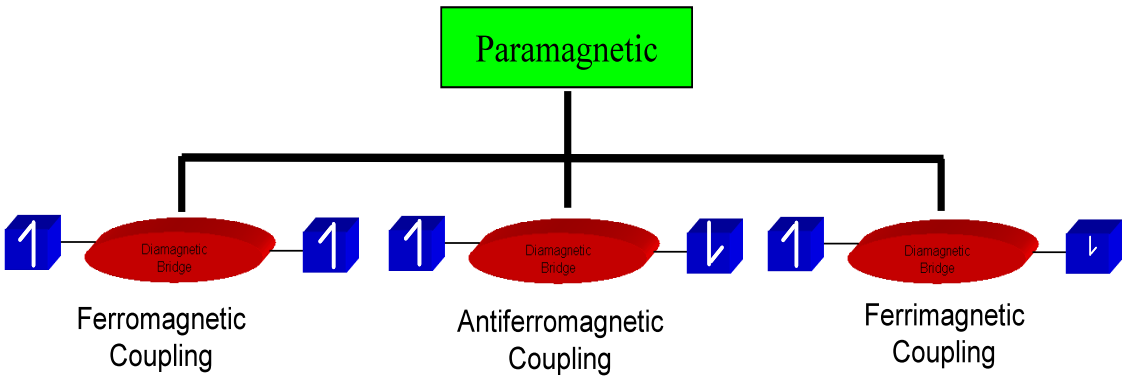

Figure I.2. Pictorial representation of three types of coupling found in paramagnetic substances

Figure I.2 depicts a few examples of the types of coupling interactions studied by magnetochemists. Molecular magnetism is the study of magnetic properties of isolated molecules. Molecular magnetic molecules can consist of one or more magnetic centers, and it is the interaction between these magnetic centers that the Shultz group desires to

understand and control. These molecules will be the building blocks for materials that exhibit bulk magnetism, which can then be incorporated into devices such as quantum computers or memory devices.

Spin-based electronics (spintronics) have received a great deal of attention over the past decade.[5] If a device is designed to read the intrinsic spin of the electron, rather than a series of ones and zeros or nuclear spins, the device will posses greater speed and higher efficiency. This increased computational speed is attributed to the relaxation time of electrons being two orders of magnitude faster than nuclear relaxations.[6] We should then be able to engineer computers that are a fraction of the size while maintaining or even increasing the current speed of processing data. Equally important is evidence indicating a significant reduction in electrical consumption to accomplish tasks using improved magnetic devices. In addition to contributing to reduced electrical generation loads for the power grid, battery powered devices could operate on significantly smaller batteries – a major consideration of human medical implants and weight/space sensitive satellite communication.[7,8,9] In order to make progress in spintronics, a few criteria must first be met. First, the system must be able to exist in two different electronic states; second, the different electronic states must be detectable; and finally, the process must be reversible.[2] All three of these criteria require some explanation.

The system must be able to exist in two different electronic states to be a viable candidate for spintronics. The "switch" required for this process is induced temporally by some external perturbation (temperature, pressure, light, etc.). A simple example of a system existing in two electronic states is illustrated by an Fe(II) complex in an octahedral field

"switching" from low spin to high spin (see Figure I.3).

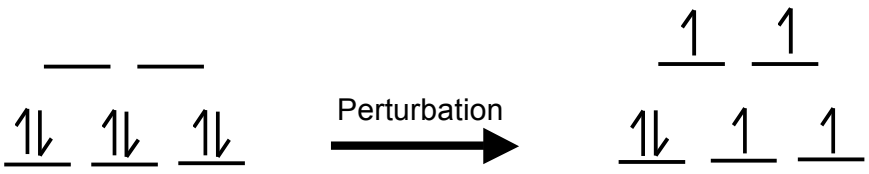

Figure I.3. Pictorial representation of a d^6 metal converting from low spin to high spin

The "switching" is required to be a process that can be induced at a desired point in time by some external perturbation. The difference between the two electronic states (whether it be high spin/low spin or any other change in electronic structure) must also be detectable, meaning that at some critical value of the perturbation there must be a drastic enough change in the system that it can be easily detected. This detection can be something as simple as a phase or color change, to something more complicated like a change in resistance. If the transition between these two states is soft and gradual, the system begins to lose desirability as a candidate for incorporation in spintronic devices.

Lastly, reversibility between the two distinct electronic states is necessary for viable computational cycling. This phenomenon was illustrated by Gütlich and coworkers, using temperature as a perturbation acting on the complex $[Fe(NH_2trz)_3](NO_3)_2$ where (NH_2trz) = 4-amino-1,2,4-triazole (Figure I.4).[10] Having different temperatures for the forward and reverse

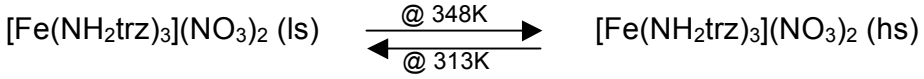

Figure I.4. Example of an Iron transitioning from low-spin to high-spin demonstrating hysteresis.

process is indicative of hysteresis, which is another desired characteristic for molecular electronics.[11,12] Gütlich uses a paramagnetic metal complex for his studies, though organic radicals are good candidates for studying unpaired electrons as well.

The Shultz group is interested in the synthesis and study of organic biradicals. Organic biradicals have several interesting properties we would like to explore. One of the most important is whether the biradical possesses a singlet or triplet ground state. A singlet state is defined as an S=0 system with the unpaired electrons aligned antiparallel, while a triplet state is an S=1 system with the unpaired electrons aligned parallel. This is illustrated using carbene as an example. Synonymous with how the electronic and atomic structure of the carbene will dictate the ground state (Figure I.5), we can use different substituents and bridges to change the electronics and conformation of our biradicals to bias the system toward different types of electron coupling.

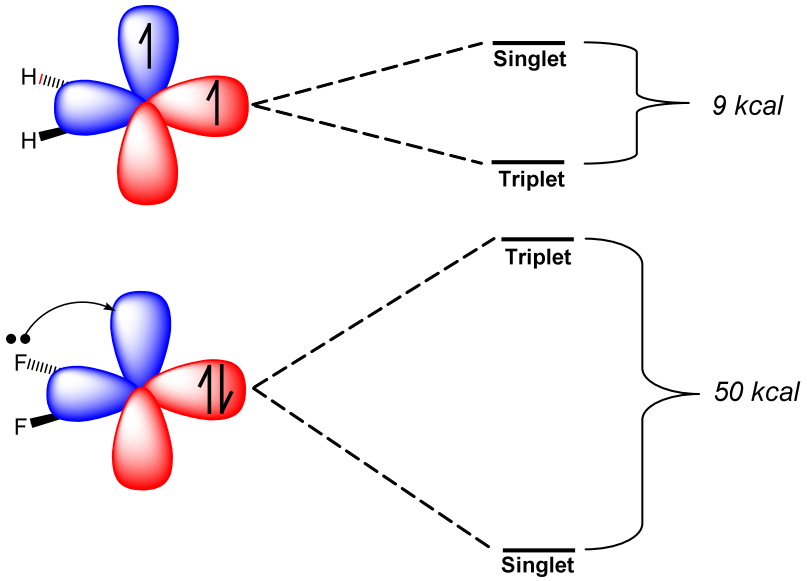

Figure I.5. CH_2 carbene (top) with triplet ground state and CF_2 carbene (bottom) with singlet ground state.[13]

When a biradical adopts a singlet ground state, it appears to violate Hund's rule. Hund's rule states that the ground state of an atom is that which maximizes spin. This violation must be taken into account and some other reason given for breaking Hund's rule. In the carbene example, electron donation from the fluorine lone pair causes the preference for the singlet state. However, a singlet ground state in some examples can be attributed to exited states mixing into the ground state, thereby stabilizing the singlet. The triplet carbene is said to be a ferromagnetically coupled system, whereas the singlet is said to be antiferromagnetically coupled (Figure I.2).

The energy difference between a singlet and triplet state is described by the exchange coupling parameter (***J***). The magnitude of ***J*** demonstrates the strength of the coupling between the unpaired electrons, and the sign of ***J*** indicates what type of interaction is present. By convention, ***J***>0 the triplet is favored, while **J**<0 the singlet is favored. The above nomenclature is a result of the HDvV Hamiltonian the Shultz group employs for their studies (Eq. 1-1).

$$\hat{H} = -2J(\hat{S}_A \bullet \hat{S}_B) \qquad (1.1)$$

Where $\hat{H}$ is the spin Hamiltonian, $\hat{S}$ is the spin angular momentum operator, and ***J***, as previously mentioned, is the exchange coupling parameter. Molecules with different ***J*** values will exhibit different magnetic susceptibilities at different temperatures. The reason for a change in the magnetic behavior is illustrated in Figure I.6. We will assume a triplet ground state with the higher energy state being a singlet. System 1 is an example with a small ***J*** which leads to population of the singlet state at low and high temperature.

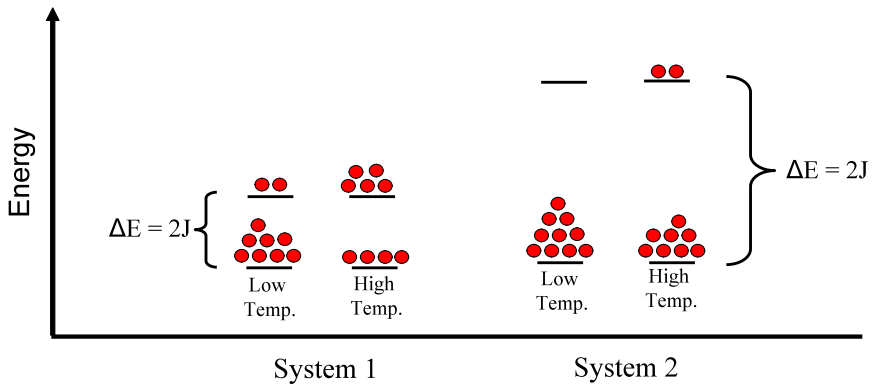

Figure I.6. Cartoon showing two-state Boltzmann distribution at high and low temperature for a weakly coupled system (system 1) and a strongly coupled system (system 2)

the singlet is densely populated. However, system 2 shows a large ***J***, therefore at low temperature there is no population of the singlet. As the temperature increases, only a small population of the singlet state is present. These different populations will manifest themselves as a change in their response to applied magnetic fields, a property we can observe.

Every material in the universe will respond to an applied magnetic field in some way.[4]

$$M = \chi \bullet H \qquad (1.2)$$

In the above equation, M is the magnetization of the sample, H is the applied field, and χ is the magnetic susceptibility. The magnetic susceptibility portion of equation 1.2 has two primary contributions: a diamagnetic and paramagnetic portion (Eq. 1.3).

$$\chi^{Exp} = \chi^{Dia} + \chi^{Para} \qquad (1.3)$$

In Equation 1.3, χ^{Dia} is the diamagnetic contribution and χ^{Para} is the paramagnetic contribution. Diamagnetism arises from paired core electrons, and all materials with paired

electrons have a diamagnetic contribution. χ^{Dia} is a negative value and is manifested by a repulsion to an external field. The most common method for determining χ^{Dia} is with the use of tabulated values of Pascal's constants (Appendix III).[14] The tabulated values and the ability to measure the experimental magnetic susceptibility leads to the calculation of the paramagnetic susceptibility by rearrangement of equation 1.3.

I.2 Magnetic Susceptibility in Shultz Group Molecules & the SQUID

In our lab, magnetic data is obtained using a Superconducting Quantum Interference Device (SQUID) magnetometer. The measurable quantity from SQUID experiments is "long moment" which is then converted to more useful values. The first is long moment converted to magnetization, from which we generate a plot of saturation magnetization (Figure I.5).

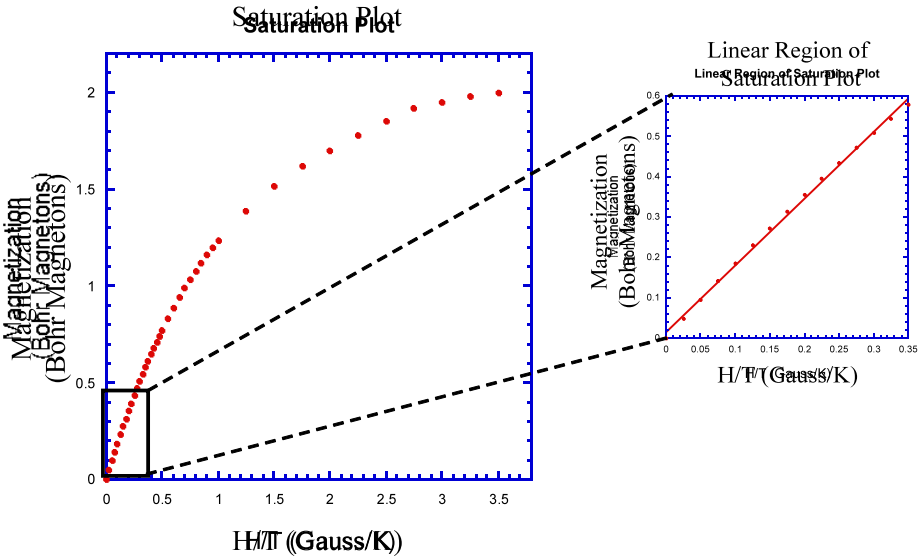

Figure I.7. Plot showing a typical saturation plot using data obtained from a SQUID magnetometer.

The saturation plot gives us two primary pieces of information:

1) The point where the curve deviates from linearity is chosen as the field for the variable temperature experiment.
2) The point of saturation tells us the number of unpaired electrons in the ground state.

After an appropriate field is chosen, a variable temperature experiment is performed to generate $\chi_{para}T$ vs. T plot. For reasons discussed previously, this plot will have curvature. Choosing an appropriate equation and fitting to this curvature will yield our exchange coupling parameter (***J***) (this is explained in greater detail in chapter 2).

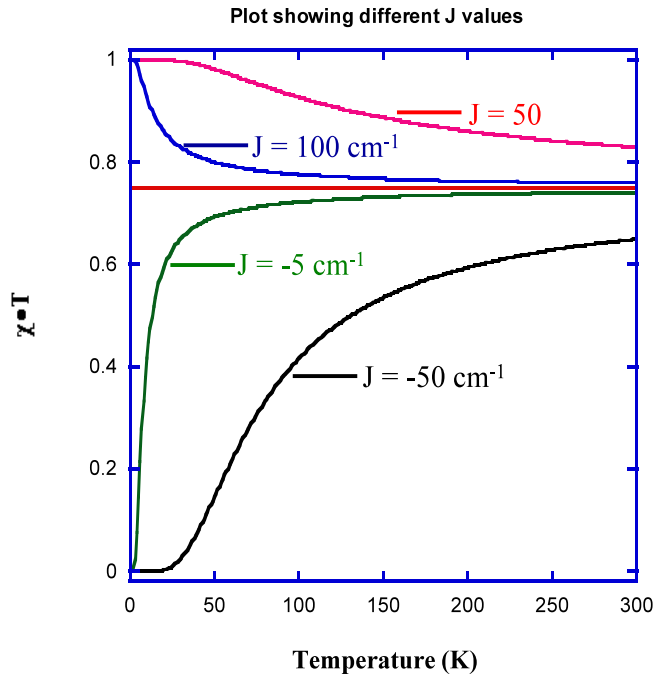

Figure I.8. Plot showing χT vs T with differing ***J*** values, horizontal red line is for an uncoupled system.

A few sentences about Figure I.6 are required. The pink and blue lines are typical for a ferromagnetically coupled system, the green and black lines are for an antiferromagnetically coupled system, and the red line is for a system that has no preference for the singlet or triplet states (i.e., ***J***=0). If we were to make ***J*** very large or very negative we would see a horizontal line (in this temperature range) at 1 and 0 respectively. The primary reason we plot $\chi \cdot T$ vs T and not χ vs T can be seen in Figure I.7.

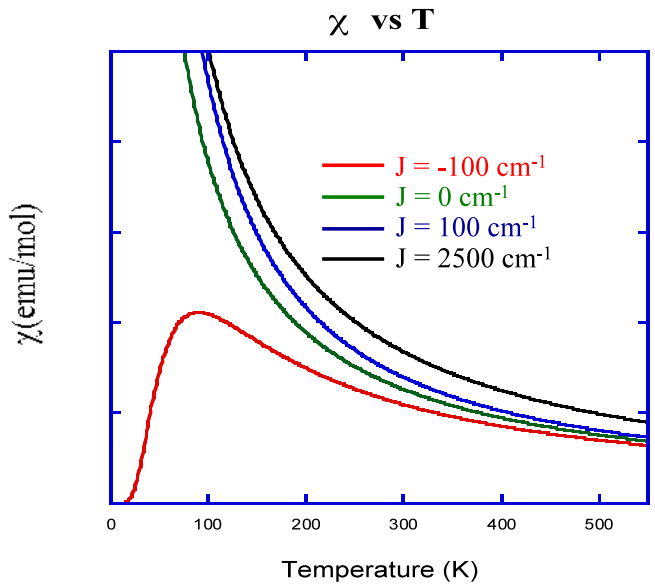

Figure I.9. Plot showing χ vs T with different ***J*** values.

The above plot demonstrates very little difference between the plots of J=0 and J=100 or even J=2500 (a substantial difference with little effect on the plot). When plotted this way, visual inspection of the data is rather difficult. The equation used to generate the above plot comes from the Curie-Weiss equation (Eq. 1.4).

$$\chi = \frac{C}{T - \Theta} \tag{1.4}$$

This equation will be discussed in much greater detail in chapter 2. In Equation 1.4, C is a constant and Θ is the Weiss constant that accounts for intermolecular interactions. When Θ>0 the intermolecular spins align parallel (i.e., ferromagnetic coupling), and when Θ<0 the spins align antiparallel.

Recall the ***J*** values discussed above are a measure of a molecules preference for one state over another (an intramolecular phenomenon), whereas Θ tells us the nature of the intermolecular interactions. When ***J*** = 0 for a biradical system, there is no preference for the singlet or triplet state. When ***J*** is large and negative, there is a strong preference for the singlet state. Conversely, when ***J*** is large and positive, there is a strong preference for the triplet state. An excellent example of molecules that have a strong preference for the singlet state is one where a bond can be formed between the unpaired electrons. Hence, a bond is nothing more than a pair of strongly coupled antiferromagnetic electrons. The singlet triplet gap for many molecules has been evaluated both experimentally and theoretically (see Table I.1).

Table I.1: List of biradicals with their corresponding experimental (top) and theoretical (bottom) ***J*** values.

Measured J Values

Molecule	J value (cm^{-1}) Reference is superscripted
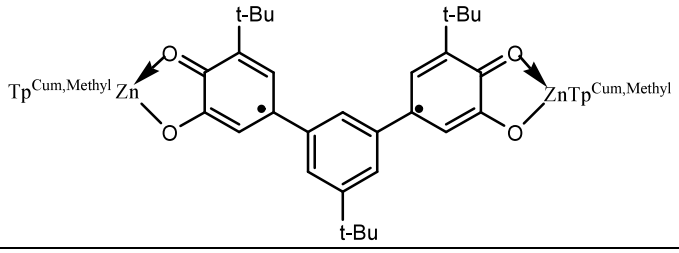	$+34.9 \pm .7^{15}$
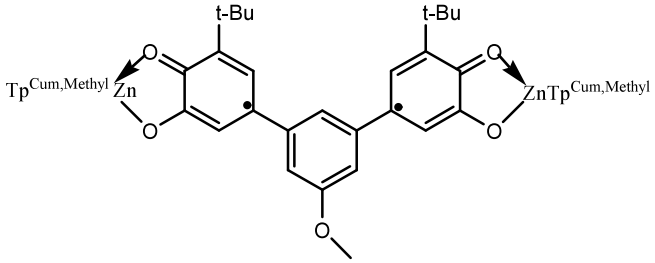	+37
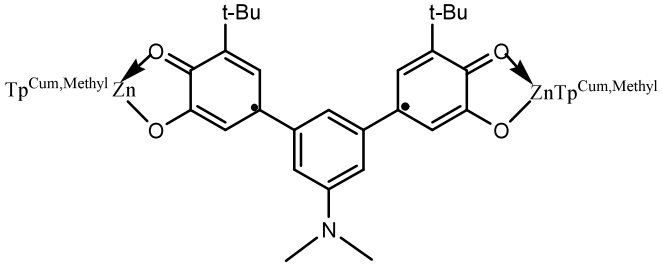	$+31.0 \pm .7^{15}$
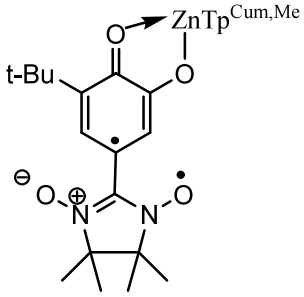	$\sim +1000^{16,17}$

Table I.1 Continued	
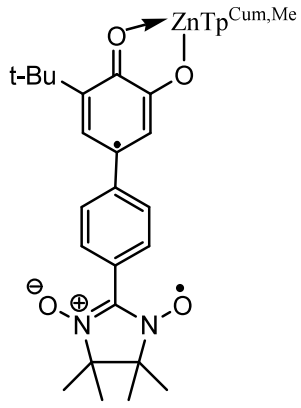	+100.0±3.2[16]
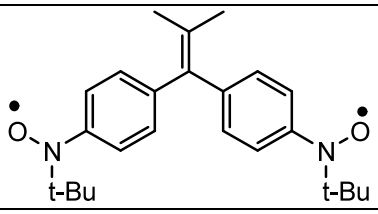	+5.3[18]
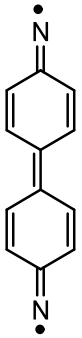	-214.3[19]

Calculated J Values

Molecule	Calculated J Value (cm^{-1})
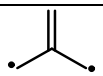	+6143.8[20]
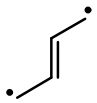	-26,540[21]
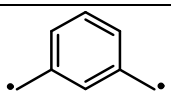	+3572[22]
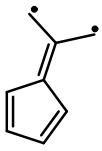	+418[23]

In looking at the table, you will notice a 2-butene biradical. Pi-bond formation for this molecule results in annihilation of the biradical. As such, the energy of this singlet triplet gap is roughly the energy of a π bond (Scheme I.1).

Scheme I.1 Resonance showing that a bond can depict a strongly AFM coupled biradical.

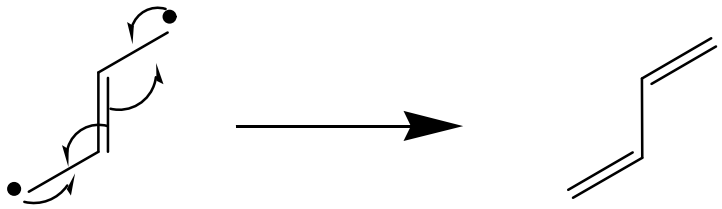

One pi bond Two pi bonds

As mentioned previously, a bond is simply a pair of strongly antiferromagnetically coupled electrons. This is important to note because if one wants to use the Longuet-Higgins "Star non-star" method to predict the coupling in a given molecule, one first must draw the resonance structure with the most possible pi bonds. The "Star non-star" method was introduced by Longuet-Higgins in the late 40's and remains a useful tool today. The following section explores the "Star non-star" method more thoroughly.[24,25,26]

I.3 Star non-star Method

The "Star non-star" method is a qualitative tool for predicting the ground state spin multiplicity of a molecule with unpaired electrons. This method is only valid for even, alternant biradicals. Stated another way, the compounds must contain an even number of atoms, and the rings contained in any of these molecules must also contain an even number of atoms (Fig I.7).

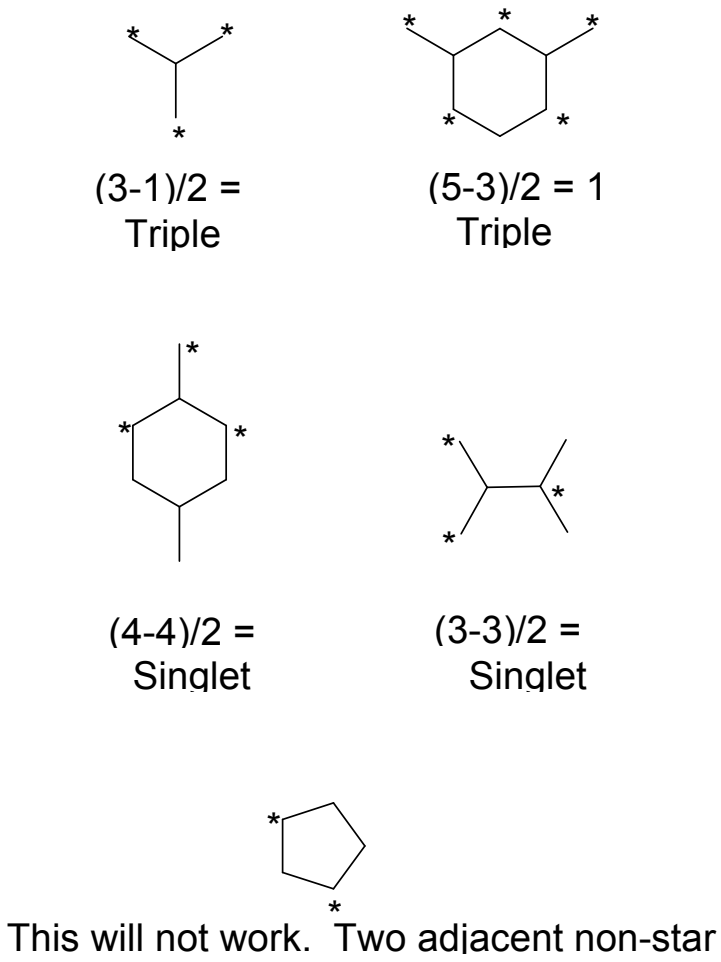

Figure I.10. Cartoon showing the utility of the star non-star method.

The process for using "star non-star" is this:

1. Draw the resonance structure with the most pi bonds possible (if the biradical is annihilated then a singlet state exists)

2. Place a star at one of the atoms then alternate star and non-star

3. Maximize the number of stars and do not place two star or two non-star atoms adjacent to each other

4. Take the # of stars less the # of non-stars and divide by 2. The resulting number is the ground state.[24]

It should be stressed the "star non-star" method is strictly qualitative and should never replace experimental evidence.

I.4 Hund's Rule

Hund's rule was mentioned previously but warrants further discussion as it relates to a molecules preference for one spin state over another. Hund's rule states, "the state of highest spin is the ground state."[27] This suggests that for a biradical, Hund's rule dictates a triplet ground state. Unlike the Pauli Exclusion Principle, Hund's rule is not a concrete requirement for placing electrons in orbitals. If a system exists that contains two electrons in two degenerate orbitals, Hund says that we must fill the orbitals so the spins are parallel.

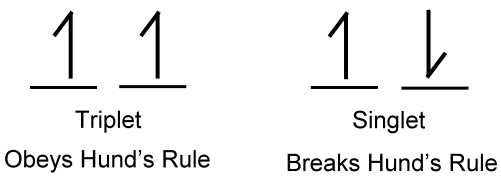

Figure I.11. Pictorial representation of molecules that obey and break Hund's rule.

The reason for this energetic preference for the triplet state is columbic in nature (See Eq I.5). In the following equation q is the charge and r is the distance separating charges.

$$E \propto \frac{q_1 q_2}{r} \qquad (1.1)$$

If electrons are placed with their spins antiparallel in a two electron two orbital system, they will be permitted to spend time in an overlap region. While occupying an overlap region, the electrons are brought closer together, thereby raising the energy of the system (or state). If

the electrons are aligned parallel, they cannot simultaneously occupy the overlap region. This is due to the Pauli Exclusion Principle, which states no two electrons can have the same 4 quantum numbers.

To zeroth order, there is no preference for the singlet or triplet state, and both states have energy of 2α (Appendix I). However, when we take the electron/electron repulsion into account, the system shows a preference for the triplet state (for the derivation of these energies see Appendix I).

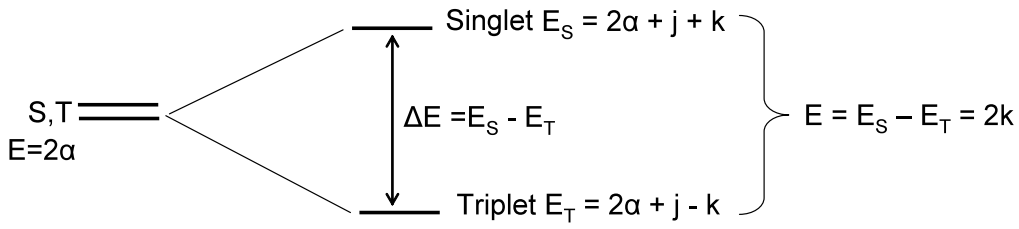

Figure I.12. Pictorial representation describing the basis of Hund's rule, please note the k term.

In the above Figure, j is the two center Coulomb integral (the electron/electron repulsion energy when two electrons are in different orbitals). This is a destabilizing energy, is identical for both states and is a positive value. The k term above is the overlap integral and is the energy of repulsion when the electrons are simultaneously in the overlap region. The k term is destabilizing for the singlet and stabilizing for the triplet (two electrons with the same spin cannot occupy the same space). This results in a 2k stabilization of the triplet and gives rise to Hund's rule.

In order to predict and understand the magnitude and mechanisms by which unpaired

electrons couple, it is imperative to understand the some fundamental principles (Hund's rule, Pauli Exclusion Principle, etc.). In the Shultz group we are interested in developing empirical models that will allow us to predict the molecular magnetic properties of molecular system. With a better understanding of magnetism at the molecular level, one could apply that knowledge to both bulk properties and single molecule magnets designed for incorporation into a vast array of electronic devices -- most notable are less power demanding computer memory components. Prior to development of these devices, research at the molecular level must be conducted.

I.5 Zero Field Splitting and Electron Paramagnetic Resonance Spectroscopy

Exchange coupled biradical complexes have unique magnetic characteristics that manifest as anomalous absorbances in EPR spectra.[28] Most notable is the dipole-dipole interaction of the unpaired electrons. The bis(Zn^{II}(SQ)$Tp^{Cum,Me}$) complexes presented herein are S=1 systems. The spin degeneracy of such systems can be calculated using 2S+1, resulting in a triplet. In the absence of an applied magnetic field, all three sublevels of the triplet state are isoenergetic. However, infinitesimally small magnetic fields generated by the unpaired electrons lift the degeneracy in the triplet manifold. The magnetic fields generated by unpaired electrons are intrinsic to the molecule; therefore, they are operative regardless of the presence or absence of an applied field. Due to the fact no external field is necessary; the degeneracy lifting has been termed zero-field-splitting (ZFS) and is described using the ZFS parameters D and E (Scheme I.2). Both D & E are anisotropic (i.e., their energies are directionally dependant), therefore the molecule must be restricted from freely tumbling in

order to observe absorbances corresponding to the ZFS parameters. [29] The bis(Zn^{II}(SQ)$Tp^{Cum,Me}$) complexes we report show D and E values (table 5) consistent with previously published results.[30,314]

Scheme I.2 Diagram showing the splitting of the formerly threefold degenerate triplet states. The ZFS parameter D is an e-/e- repulsion energy and describes the deviation from cubic symmetry. E is commonly referred to as the rhombic parameter and is a measure of the molecules deviation from axial symmetry.[5]

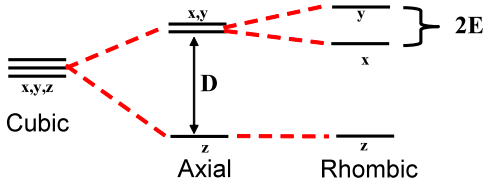

EPR spectrum. ZFS information is obtained by collecting the EPR data in a frozen matrix or a powder sample. Electron charge density is roughly three orders of magnitude greater than the charge density found at the nucleus. Consequently, electron-electron interactions (i.e., dipole-dipole interactions) are the dominant interaction for EPR data collected in both frozen matrices as well as powder samples. In contrast, hyperfine interactions are the dominant feature in fluid solution EPR spectra at room temperature. The random tumbling of molecules in a fluid causes a zeroing of the dipolar interactions, making way for hyperfine interactions to dominate the spectra.

In addition to ZFS parameters, compounds containing more than one unpaired electron exhibit an additional unique spectroscopic feature. In a system containing 2 antiferromagnetically coupled electrons, the feature is referred to as the $\Delta m_s=2$ transition. The $\Delta m_s=2$ transition violates the spin selection rules of EPR ($\Delta m_s=0$ & $\Delta m_I=1$). [32] The

spin forbiddenness of the transition results in a "weak" absorbance. Sample preparation is paramount when collecting data on ZFS parameters and $\Delta m_s=2$ transitions to ensure visualization of the weak and often complex spectra generated during the above experiments.

Chapter II

Hyperfine Interaction, Spin Polarization, and Spin Delocalization as Probes of Donor-Bridge-Acceptor Interactions in High-Spin Biradicals

(Portions of this section have been published: *J. Phys. Chem. B* **2010,** *114,* 14712–14716) [33]

II.1 ABSTRACT

Computations and EPR spectroscopy are used to probe the spin distribution of donor-bridge-acceptor (D-B-A) biradical complexes: $Tp^{Cum,Me}Zn$(SQ-NN)Zn (**1**), $Tp^{Cum,Me}Zn$(SQ-1,4-Ph-NN) (**2**), $Tp^{Cum,Me}Zn$(SQ-2,5-TP-NN) (**3**) and $Tp^{Cum,Me}Zn$(SQ-2,5-Xyl-NN) (**4**) (SQ = orthosemquinone and NN = nitronylnitroxide). These complexes are ground-state analogs of the charge-separated excited states formed in photoinduced electron transfer reactions. The ferromagnetic intraligand magnetic exchange interaction in these complexes is mediated by the bridges and stabilizes the triplet ground states of these molecules. Detailed spectroscopic and bonding calculations have been used to elucidate the role of the bridge fragment (B) and its conformation relative to donor (SQ) and acceptor (NN) on spin density distribution. The computed results correlate well with experimental nitrogen hyperfine coupling constants.

II.2 INTRODUCTION

Static and dynamic distortions that result in non-planar geometries for π delocalized donor-bridge-acceptor (D-B-A) systems can have a dramatic impact on the ability of the bridge fragment to facilitate electron transfer/transport over long distances.[47-54,8] For example, in nonadiabatic photoinduced electron transfer (PET) processes, photoexcitation

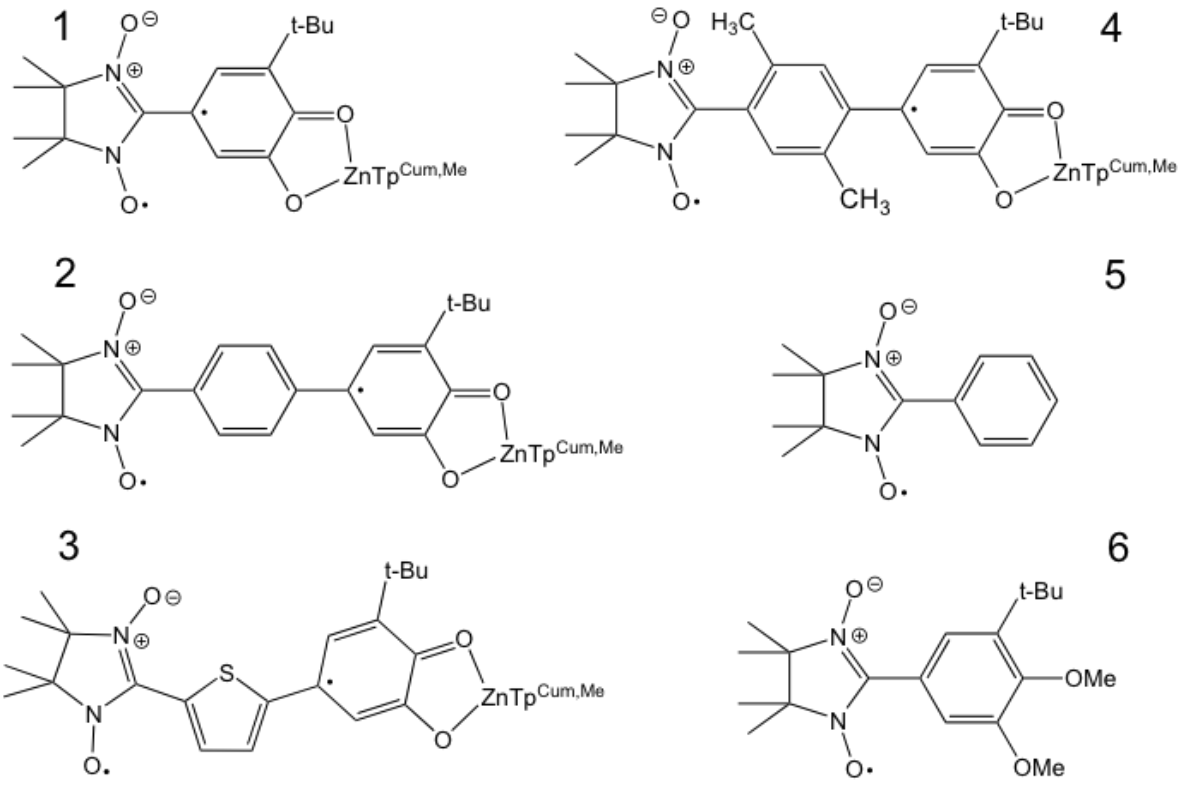

Figure II.1 Radical and Biradical molecules

of D yields a D*-B-A excited state which can undergo facile electron transfer to form a spin singlet biradical D^{+}-B-A^{-} charge separated state.[42] The singlet-triplet gap (2***J*** where ***J*** is the exchange parameter) of the charge separated excited state is determined by the effect of

applied magnetic fields on decay rates.[43,44] The exchange parameter is then used to evaluate the electronic coupling matrix element ($\boldsymbol{H_{ab}}$) for a given D-B-A system.[54,55,11] During our study of mechanisms of exchange- and adiabatic electronic coupling we have developed covalently linked, nondisjoint heterospin triplet D-B-A biradicals thatcan be described as *ground state analogues* of these photogenerated triplet charge separated states.[48, 53, 58, 57, 13] In these studies, a perturbative valence bond configuration interaction (VBCI) model that utilizes spectroscopic and magnetic observables was used to understand the electronic origin of both H_{ab} and the strong ferromagnetic couplinginthe NN-SQ (SQ-B-NN) D-B-A biradical series, $Tp^{Cum,Me}M$(SQ-B-NN)[59, 15]

Wasielewski has suggested that a potentially important mechanism for controlling or modulating charge recombination dynamics in D-B-A charge separated states occurs through the spin density distribution on the bridge fragment.[9] Some of the key questions in molecular electron transfer/transport focus on the magnitude of the electronic coupling in the D-B-A fragment, molecular distortions that are coupled to the charge separated state, and the intimate electronic structure of the bridge moiety in a D-B-A system. In this study, we attempt to address the nature of the spin density distribution in ground-state triplet D-B-A biradical ligand complexes using a combination of EPR spectroscopy and detailed calculations that probe the effects of the bridge and its conformation. These studies provide detailed insight into the relationship between the degree of D→A charge transfer, the nature of the bridge fragment, and key geometric distortions and the spin density distribution in the D, B, and A fragments. We find that direct measurement of the specific isotropic hyperfine interaction parameters in D-B-A biradicals that employ a NN acceptor provide key insight

into the electronic origin of the spin density distribtion triplet D-B-A biradicals, and serve as important *ground state probes* of excited state contributions to spin delocalization, spin polarization, charge transfer, and non-planar D-B-A distortions.

II.3 EXPERIMENTAL

Electron Paramagnetic Resonance Spectroscopy. Fluid solution X-band EPR spectra were recorded at room temperature on an IBM-Brüker E200SRC continuous-wave spectrometer at room temperature. Samples were dissolved in CH_2Cl_2 solution (ca. 0.2 mM) and spectra collected in quartz sample tubes. The resultant isotropic EPR spectra were simulated using the programs XSophe and EasySpin to obtain accurate isotropic nitrogen hyperfine coupling constants (a_N). The complexes $Tp^{Cum,Me}$Zn(SQ-NN) **1** and $Tp^{Cum,Me}$Zn(SQ-1,4-Ph-NN) **2**, ($Tp^{Cum,M}$ = hydro-tris(3-cumenyl-5-methylpyrazolyl)borate; NN = nitronyl nitroxide; SQ = semiquinone; 2,5-TP = thiophene; 1,4-Ph = phenylene; 2,5-Xyl = *para*-xylyl; Scheme 1) possess ferromagnetically exchange coupled biradical ligands that possess a total spin of $S_T = 1$. Molecules $Tp^{Cum,Me}$Zn(SQ-2,5-TP-NN) **3**, and $Tp^{Cum,Me}$Zn(SQ-2,5-Xyl-SQ) **4** are also non-disjoint biradicals and are also anticipated to possess $S_T = 1$ ground states. The nitronyl nitroxides NN-Ph (**5**) and NN-Ph(OMe) (**6**) are monoradicals and possess $S_T = 0.5$. Spectra were fit assuming a hyperfine splitting due to two, equivalent I = 1 N nuclei and a line shape model possessing an angular dependence on g and Gaussian line shapes. The magnitudes of the isotropic hyperfine splitting as well as the line widths were adjusted accordingly to fit the experimental spectra. Hyperfine values were simulated with a confidence of 0.5 x 10^{-4}cm^{-1}. For the S = 1 donor-acceptor systems, the relationship

$$a_{N(S=1)} = a_N / 2$$

has been used to relate the measured N hyperfine coupling constant of the S = 1 pair state ($a_{N(S=1)}$) in the strong exchange limit ($J >> a_{N(S=1)}$) to the intrinsic NN isotropic hyperfine coupling constant (a_N).

Electronic Structure Calculations. Spin unrestricted gas-phase geometry optimizations for all compounds were performed at the density functional level of theory using the Gaussian 03W software package.[16] Calculations for molecules **1**-**4** were performed on the S_T = 1 spin triplet ground state, while those for monoradicals **5**-**6** were performed on the spin doublet ground state. All calculations were performed on neutral molecules and employed the B3LYP hybrid exchange-correlation functional. A631G(d,p) basis set, a split valence basis set with added polarization functions, was used for all atoms. Input files were prepared using the molecule builder function in the

Gaussview software package. Ground state optimized geometries were calculated with dihedral angles between the nitronyl nitroxide and phenyl rings, or the phenyl and semiquinone rings of **2** varying between 0 and 180 degrees in steps of 15° in order to determine the effects of bond torsions on spin density distrubitions. In these calculations, the SQ-B and B-NN dihedral angles were held fixed, and all remaining coordinates were allowed to optimize to the lowest energy geometry using the Berny algorithm. Mulliken spin populations were extracted from the resulting output file.

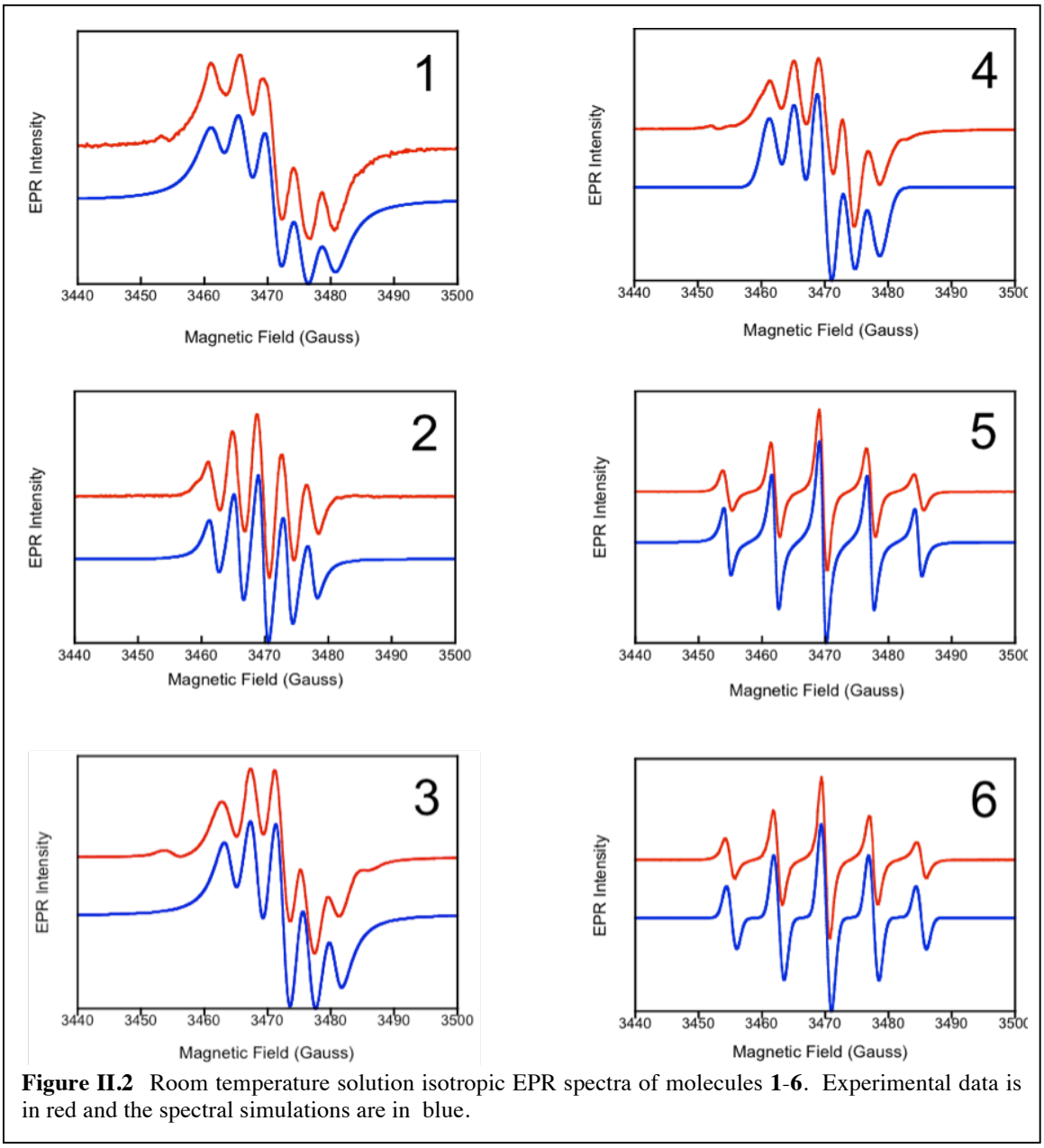

Figure II.2 Room temperature solution isotropic EPR spectra of molecules **1**-**6**. Experimental data is in red and the spectral simulations are in blue.

II.4 RESULTS AND DISCUSSION

Electron Paramagnetic Resonance Spectroscopy. The room temperature solution EPR spectra for molecules **1**-**6** are presented in Figure II.2 (blue) along with their spectral simulations (red). Here, molecule **1** is a D-A biradical, molecules **2**-**4** are D-B-A biradicals,

and molecules **5**-**6** are B-A monoradicals. The biradical molecules **1**-**4** all possess high-spin $S_T = 1$ ground states due to ferromagnetic exchange coupling between the NN and SQ radicals.[2, 8, 13] All biradical spectra are observed to be in the strong exchange limit with the isotropic Heisenberg-Dirac-vanVleck (HDvV) exchange parameter, $\boldsymbol{J}$, being much greater than the N hyperfine interaction (*hfi*). The resonance line for **1**-**6** is centered at the free electron *g*-value (g_e) and split into five lines due to the *hfi* with the two equivalent, or very nearly equivalent N nuclei associated with the nitrogen atoms of the nitronyl nitroxide acceptor radical. The isotropic N hyperfine parameters obtained by spectral simulation for molecules **1**-**6** are listed in Table 1.

Table II.1 Isotropic NN nitrogen *hfi* parameters for molecules **1**-**6**.

	1	**2**	**3**	**4**	**5**	**6**
$\lvert a_N \rvert$ (10^{-4}cm^{-1})	7.60 +/-0.05	7.20 +/- 0.05	7.38 +/- 0.1	6.74 +/-0.05	7.06 +/- 0.05	7.07 +/- 0.05
Line width (10^{-4}cm^{-1})	2.1	1.1	1.9	1.7	0.9	0.9

$g \sim g_{\text{free electron}}$

Table II.2 Calculated dihedral angles for molecules **1**-**6** (full unconstrained geometry optimization).

Dihedral angle (º)	NNPh (**5**)	NNThioSQZnTp (**3**)	NNPhSQZnTp (**2**)	NNSQZnTp (**1**)	NNPh(MeO)$_2$ (**6**)	NNPh(CH$_3$)$_2$SQZnTp (**4**)
Bridge-Acceptor	6	0	1	3[1]	6	46-51
Donor-Bridge	n/a	0	31-32	n/a	n/a	47-48

[1] donor-acceptor dihedral

The experimentally determined a_N values for molecules **1**-**6** reflect the effects of D→A charge transfer, spin polarization, and spin delocalization on the spin density distribution in

these molecules. We have performed full DFT geometry optimizations on molecules **1**-**6** and the optimized dihedral angles between the D-B and B-A are given in Table 2. Note the remarkable B-A planarity calculated for all of the molecules except for xylyl bridged **4**, indicating an electronic driving force for a high degree of B-A interaction in the absence steric constraints. Interestingly, for D-B-A molecule **3**, which possesses a thiophene bridge, the calculated ground state geometry is *planar*, while the phenylene bridge in **2** is quite distorted from planarity. In order to develop a greater understanding of the spin density distrubutions in these molecules, we have calibrated the results of DFT spin density calculations at these optimized geometries to the experimental a_N *hfi* parameters. This is shown in Figure II.3, where the calculated spin density per N on the NN fragment (ρ_N) is plotted as a function of the experimental isotropic N *hfi* parameter a_N. The observed linear behavior follows the expected relationship $a_N = Q\rho_N$,[17, 18] which was first described by McConnell, and suggests that these calculations can adequately predict the proper trends in spin density distrubution for molecules **1**-**6**, and provide

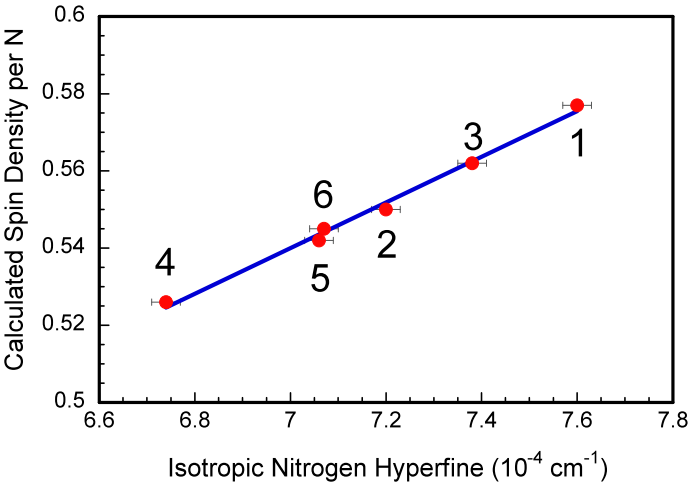

Figure II.3 Calculated spin density per NN nitrogen as a function of the isotropic N *hfi* (a_N) for molecules **1**-**6**. The blue line is a best-fit line through the six data points.

strong support for the calculated gas phase geometries dominating in solution. It is clearly evident from Figure II.3 that donor interactions, the nature of the bridge fragment, and D-B/B-A ring torsions conspire to modulate the N *hfi* on the NN acceptor, indicating that the N *hfi* can serve as a sensitive probe of D→A charge transfer, spin polarization, and spin delocalization in D-A and D-B-A molecules.

Molecular Orbital Description of Donor-Acceptor Interactions and Spin Delocalization. In order to develop greater insight into the electronic and geometric origins of the experimental isotropic N *hfi*, the calculated spin density distributions on the Donor, Bridge, and Acceptor, and the spin populations on the NN nitrogen and bridging carbon atoms, we will utilize a qualitative molecular orbital (MO) diagram for phenylene bridged **2** that is based on the results of our bonding calculations. The MO diagram is presented in

Figure 3, and displays key SQ, Ph, and NN frontier molecular orbital interactions. The phenylene e_1 orbital possesses the proper symmetry to mix with the SQ(π) singly occupied molecular orbital (SOMO) and the NN(π*) lowest unoccupied molecular orbital (LUMO). Strong orbital mixing between the NN(π*) and Ph(e_1) orbitals results in an energetically stabilized NN-Ph(π*-e_1) bonding MO that allows for greater interaction with the SQ SOMO. From this figure, it is easy to see how occupation

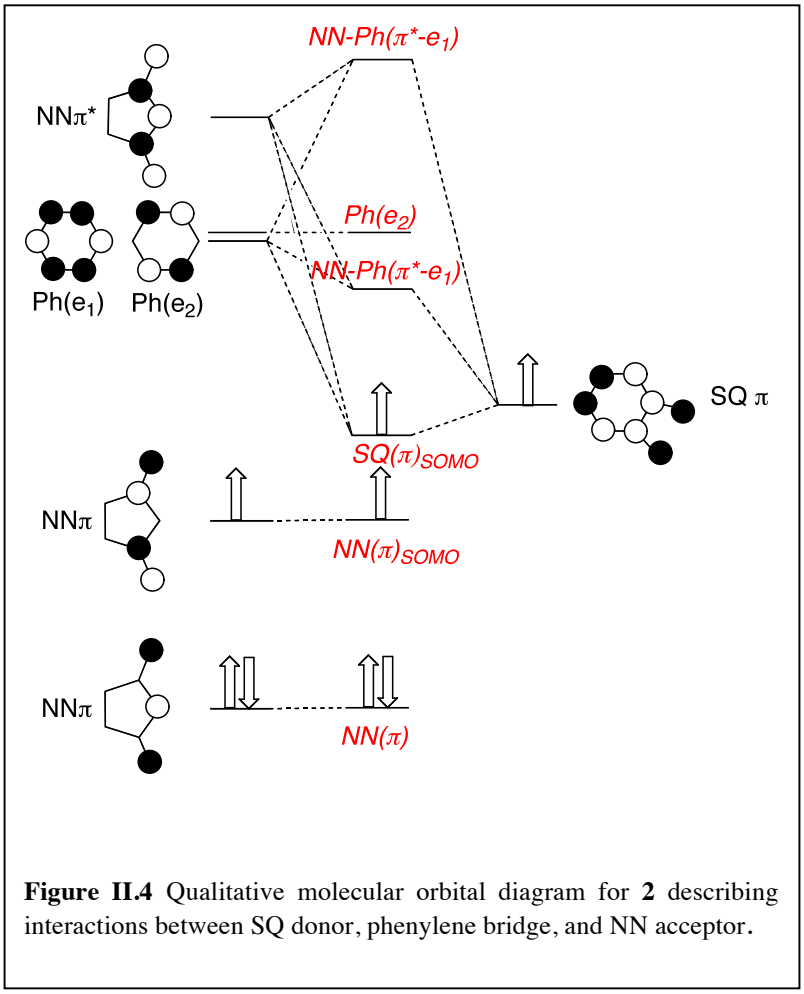

Figure II.4 Qualitative molecular orbital diagram for **2** describing interactions between SQ donor, phenylene bridge, and NN acceptor.

of the $SQ(\pi)_{SOMO}$ allows for positive spin density to be transferred from the SQ donor the the phenylene bridge and the NN nitrogens via a spin delocalization mechanism. A planar D-B-A bridge geometry, as calculated for thiophene bridged **3**, will result in a markedly stronger transfer of positive spin density from the SQ donor to the bridge and NN acceptor fragment. This effect is observed experimentally for **3** which possesses the largest a_N value for any of the three D-B-A systems detailed in this study (Figure 2 and Table 1). However, bond torsions that reduce the D-B and/or B-A π conjugation will dramatically reduce $SQ(\pi)$-$Ph(e_1)$ and $Ph(e_1)$-$NN(\pi^*)$ overlap, a_N, and the transfer of positive spin density to the bridge and acceptor. This is observed experimentally for phenylene bridged **2** and xylyl bridged **4**, which possess markedly reduced a_N values compared with **3** (Figure II.4).

We have calculated the spin densities on the NN, phenylene, and SQ fragments of models for molecule **2** in limiting geometries in order to ascertain the relative effects of D-B and B-A interactions in D-B-A biradicals, and the results are presented in Table 3. In the first geometry, the phenylene bridge is orthogonal to both the SQ donor and the NN acceptor ($\overline{D}$-B-$\overline{A}$; overbar indicates 90° rotation from planar geometry) with the expected result that the now isolated NN and SQ radicals possess spin densities that approach unity. In the D-B-$\overline{A}$ geometry, the phenylene bridge is orthogonal to the NN acceptor resulting in ~9% of the SQ spin density being transferred to the phenylene bridge, while the planar D-B-A geometry yields increased B and A spin density with a remarkable 20% reduction in positive spin density on the SQ donor, underscoring the strong D→A interaction in the fully planar geometry that facilitates spin delocalization. Interestingly, in the

Table II.3 Calculated spin densities for molecule **2** as a function of D-B and B-A bond torsions.

Net Calculated Spin Density on NN, Phenylene, SQ			
NN	*Phenylene*	*SQ*	*Geometry*
0.996	0.011	0.993	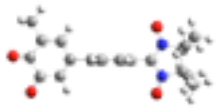 $\overline{D}-B-\overline{A}$
0.998	0.093	0.909	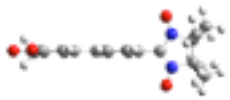 $D-B-\overline{A}$
1.047	-0.041	0.994	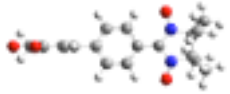 $\overline{D}-B-A$
1.124	0.072	0.804	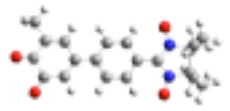 $D-B-A$

$D-\overline{B}-\overline{A}$ geometry, positive spin density on the NN acceptor increases but now negative spin density resides on the phenylene bridge. In order to better understand the origin of negative spin density on the bridge fragment, we now focus on the calculated spin populations for the NN nitrogen atoms and the NN bridging carbon atom as a function of donor, bridge, and acceptor rotations from planarity (Figure 4). Here, it is observed that ρ_N and ρ_C basically track one another with individual NN acceptor and phenylene bridge rotations away from the planar geometry. The similar tracking occurs because both of these rotations disrupt B-A communication. The apparent divergent behavior in ρ_N and ρ_C at planar geometries can be explained using Figure II.5. In a planar geometry, D→A charge transfer is maximized, and there is maximal overlap between the SQ(π), Ph(e_1), and NN(π*) functions resulting in a $SQ(\pi)_{SOMO}$ molecular orbital delocalized over all three fragments. This effectively increases the positive spin density on the NN by spin delocalization onto the

N and C atoms of the NN(π^*) orbital. This has the effect of increasing the positive spin population on the NN nitrogen atoms as well as the bridging carbon due the the large atomic orbital coefficients on these atoms in the NN(π^*) orbital. Conversely, when the phenylene bridge and the NN acceptor are orthogonal, the spin populations on NN resemble those of the isolated NN radical, with a large negative spin population on the NN bridging carbon due to spin polarization and a less positive spin population on the NN nitrogen atoms due to the reduced spin delocalization from the SQ donor. Finally, when the donor is rotated out of the plane, spin delocalization via D→A charge transfer is minimized. The negative spin density on the phenylene bridge and the increased positive spin density on the NN acceptor is a result of enhanced spin polarization that results from a NN(π)→ NN-Ph(π^*-e_1) charge transfer

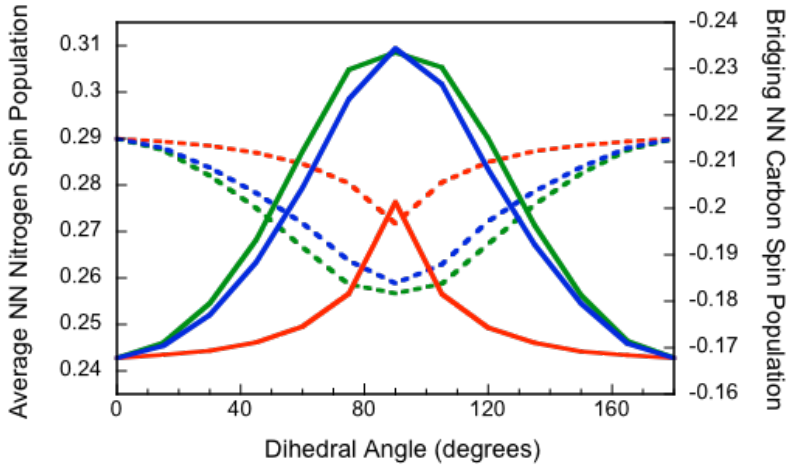

Figure II.5 Dashed lines are calculated spin populations on the NN nitrogen and solid lines are bridging C for a computational model of **2**. Calculations were performed with the donor-bridge-acceptor motif where: donor = SQ(red), bridge = phenylen (green) and acceptor = NN (blue) each individually rotated from the planar D - B - A geometry.

state. The strong interaction between the NN(π) and Ph(e_1) orbitals when these groups are planar stabilizes the NN-Ph(π^*-e_1) orbital leading to a smaller ΔE term in the perturbative configuration interaction expression that leads to a negative spin population on the NN bridging carbon atom. These results indicate that direct measurement of the isotropic N and C *hfi* in D-B-A biradicals that employ a NN acceptor will provide considerable insight into the electronic origin of the spin density distribution in D-B-A biradicals, and serve as a *ground state probe* of excited state contributions to spin delocalization, spin polarization, charge transfer, and non-planar D-B-A distortions.

II.5 CONCLUSIONS

We have shown that EPR determined hyperfine coupling constants, evaluated in the context of detailed bonding calculations, can effectively describe how spin density distributions can be used to evaluate electronic/exchange interactions in D-B-A biradicals. In addition, the spin density distributions were used to probe molecular conformation and the degree of D→A charge transfer. Our results indicate that NN_{LUMO}-$Bridge_{LUMO}$ interactions are most critical for strong D-B-A interaction in **1**-**4**. Further studies are underway to experimentally evaluate these predictions.

Chapter III

Synthesis of and Structure-property Relationships in Zinc Complexes of bis-metaphenylene Semiquinone Biradical Species

(Portions of this section have been published: *J. Phys. Org. Chem. B* **2011**)[60]

III.1 Abstract

The design of novel, functionalized bis-metaphenylene semiquinone (SQ) ligands and their corresponding metal complexes which combine conformational flexibility and electron-withdrawing, electron-donating, and electroneutral substituents enable investigation of multiple structure-property relationships. Along these lines, we report the synthesis of three new bis(Zn^{II}(SQ)$Tp^{Cum,Me}$) complexes containing the bis-metaphenylene coupling fragment. Using both electron paramagnetic resonance spectroscopy and SQUID magnetometry, we show how spin-density is affected by the bis-metaphenylene system substituents.

III.2 Introduction

New paramagnetic ligands are of general interest in both organic and inorganic chemistry as components of sensors, switches, and molecular spintronics.[61-65, 8] Previous research in our group has shown that both conformation and substituents can modulate spin density and exchange coupling in Bis(Zn^{II}(SQ)$Tp^{Cum,Me}$) biradical ligand complexes.[65,66] The design of novel, functionalized semiquinone (SQ) ligands containing electron-withdrawing, electron-donating, and electroneutral substituents enables investigation of multiple structure-property relationships and building blocks for new materials. In an effort to analyze the nature of the substituent effects observed in the bis(Zn^{II}(SQ)$Tp^{Cum,Me}$) complexes, a broader range of substituents was required to round out the series initially studied by us, where X= *t*-Bu, $N(CH_3)_2$, and NO_2. Therefore, the unsubstituted case (X=H) was prepared as a reference, an electroneutral substituent (X=Ph) was selected, as well as the π-electron donor/σ-acceptor substituent ($X=OCH_3$). See Figure 1.

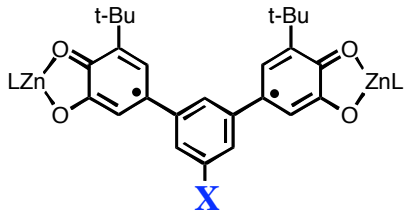

X= *t*-Bu, $N(CH_3)_2$, and NO_2, H, Ph, OCH_3
L= 3-cumenyl-5-methyl hydrotris-pyrazoloborate

Figure III.1 Substituted bis(Zn^{II}(SQ)$Tp^{Cum,Me}$) complexes.

III.3 Results and Discussion

Synthesis.

To acquire these new ligand species and zinc complexes, the synthetic strategy shown in Scheme 1 was employed. Yields at each step are provided.

Scheme III.1 Bis(Zn^{II}(SQ)$Tp^{Cum,Me}$) Complex Synthetic Sequence.

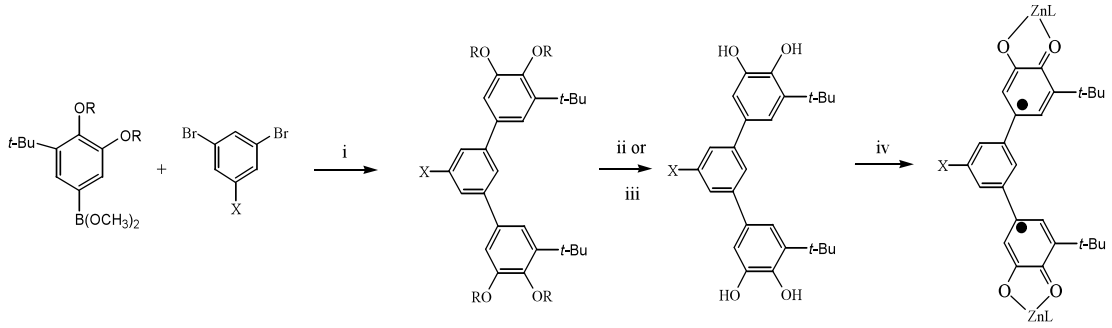

3a-c **4a-c** **5a-c**[b]

		% Yield	% Yield	% Yield
1a ($R=CH_3$)	**2a** (X=H)	73	91	83
1a ($R=CH_3$)	**2b** (X=Ph)	60	93	83
1b (CH_2OCH_3)	**2c** ($X=OCH_3$)	75[a]	95	77

Conditions: i: Boronic Ester (2eq), phenyl halide (1eq), $Pd(PPh_3)_4$ (5-14 mol%), C_2H_5OH (6-15mL), 2M Na_2CO_3 (9-18mL), THF (50mL), reflux (20-30h). ii: BBr_3 (3-4eq), CH_2Cl_2 (20mL), -78°C→RT, 18h. iii: CH_3OH (45mL), HCl (0.1mL), reflux (24h). iv: (1) $Zn(ClO_4)_2{\cdot}6H_2O$ (2eq), $KTp^{Cum.Me}$ (2eq), CH_3OH (4.5mL), CH_2Cl_2 (30mL), (0.5-1h); (2) $N(C_2H_5)_3$ (1.5h); (3) open to air, 18h, RT.
Notes: [a]Satisfactory conversion required addition of another aliquot of Pd catalyst and base after 24h. [b]$L=Tp^{Cum,Me}$

The bis(Zn^{II}(SQ)$Tp^{Cum,Me}$) complexes were prepared using proven synthetic methodology:[1] (1) Suzuki coupling to form compounds **3a-c**, (2) deprotection to the catechols **4a-c** and (3) complexation to form compounds **5a-c**. Full details of the experimental procedures are found in the supplemental material.

Characterization of the Bis(Zn^{II}(SQ)$Tp^{Cum,Me}$) Complexes.

The bis(Zn^{II}(SQ)$Tp^{Cum,Me}$) complexes **5a-c** were characterized by several means. Absorptions in the infrared spectra readily identify the $Tp^{Cum,Me}$ ligand (~2540 cm^{-1}, ν_{B-H}) and the SQ (~1450 cm^{-1}, $\nu_{C=O}$) functionality. Also, observation of an n →π* transition from

10,000-15,000 cm^{-1} in the ultraviolet-visible spectra[1] verifies the SQ moiety. The triplet biradical complexes were readily identified by EPR. SQUID magnetometry measured the magnetic susceptibility of the complexes, from which values for ***J*** were calculated. Finally, x-ray crystallographic data confirm the structures of the complexes.

Spectroscopy

Infrared and UV-Vis absorptions of the bis(Zn^{II}(SQ)$Tp^{Cum,Me}$) complexes prepared in Scheme 1 were found to be consistent with those reported earlier.[1] Critical absorption energies are shown below in Table III.1.

Table III.1 IR and Electronic Absorption frequencies for Bis(Zn^{II}(SQ)$Tp^{Cum,Me}$) Complexes.

	Infrared		UV-Vis
Compound	B-H Frequency	SQ Frequency (cm^{-1})	n→π* transition
5a	2536	1440	13,086
5b	2547	1440	13,080
5c	2547	1439	14,060

EPR measurements on the bis(Zn^{II}(SQ)$Tp^{Cum,Me}$) complexes were taken at 77K for the Δm_s=1 transition and 298K for the Δm_s=2 transition. Shown in Figure 2 are the results of EPR experiments. Immediately above each experimental spectrum was the simulated spectrum obtained via the WINEPR Simfonia fitting program.[63] The experimental spectra are in agreement with the simulations and are also consistent with spectra obtained from bis(Zn^{II}(SQ)$Tp^{Cum,Me}$) complexes reported earlier.[1] These findings, when taken together, suggest successful formation of triplet bis(semiquinone) biradical species. In the case of **5b**, it was unclear as to why the transition was broadened.

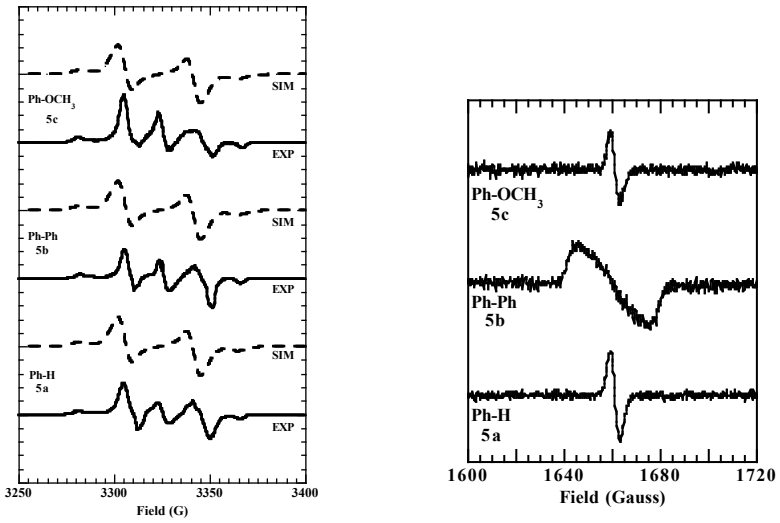

a. $\Delta m_s = 1$ transition (77K). b. $\Delta m_s = 2$ transition (298K).

Figure III.2 Bis(Zn^{II}(SQ)$Tp^{Cum,Me}$) EPR $\Delta m_s = 1$ and $\Delta m_s = 2$ transitions.

III.4 Magnetometry

SQUID magnetometry measurements were carried out to ascertain both the maximum spin (saturation) values (M_{sat}) and the dependence of the complexes' molar magnetic susceptibility (χ_M) on temperature as a function of substituent. For these biradicals, we observed M_{sat} to approach a maximum value of 2.0 Bohr magnetons (Figure 3), corresponding to two unpaired electrons, as the magnetic field strength was increased at ~4K. Likewise, χ_M •T values were observed to approach their maximum value of 1.0 emu•K/mol at low temperature, where population of the higher energy singlet state does not occur to a large extent. As the temperature was raised during the experiment, increasing population of the higher lying singlet state reduced the triplet contribution to χ_M, causing χ_M •T values to approach 0.75 emu•K/mol. These findings are consistent with earlier SQUID magnetometry data collected on analogous compounds.[1] Strength of exchange coupling can be determined

by fitting the magnetic data to a field-independent van Vleck expression (using $H = -2\boldsymbol{J}\hat{S}_1 \cdot \hat{S}_2$), Equation 1,[4,5]

$$\chi T = \frac{2Ng^2\beta^2}{k\left[3 + e^{-2J/kT}\right]} \qquad \textbf{Eq. 1.}$$

where g was the isotropic Landé constant ($g = 2.0023$), β was the Bohr magneton, T was the temperature in Kelvin, k was Boltzmann's constant, $\boldsymbol{J}$ was the intramolecular exchange coupling parameter ($2\boldsymbol{J} = \Delta E_{ST}$), and $\hat{S}_1$ and $\hat{S}_2$ are the spin operators for the semiquinones. The decrease of the χT data at very low temperatures (below 5K) was accounted for with a Weiss correction, using the expression $\chi_{eff} = \chi/(1 - \vartheta\chi)$, where $\vartheta = 2zJ'/(Ng^2\beta^2)$.[64] The origin of J' can be zero-field splitting, intermolecular interactions, saturation effects, or some combination of these.[7] The fit results are seen in Table III.2. For comparison, values for complexes prepared by Bodnar are also included.

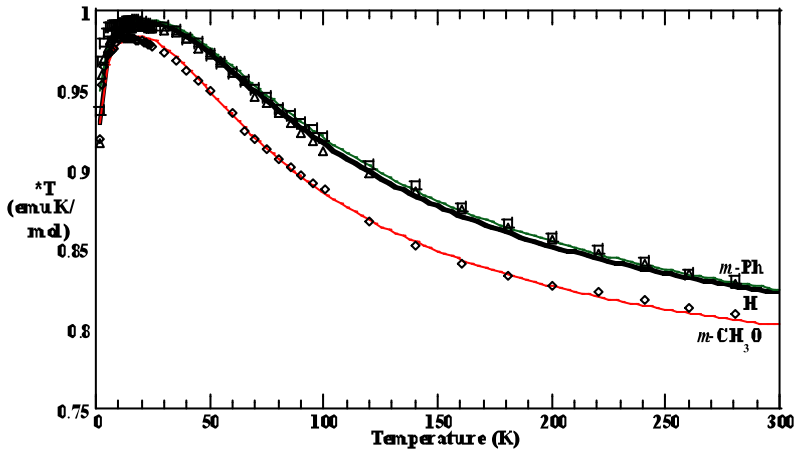

Figure III.3 Bis(Zn^{II}(SQ)$Tp^{Cum,Me}$) Complex χT versus T.

Table III.2 Bis(Zn^{II}(SQ)$Tp^{Cum,Me}$) Complex Exchange Coupling Parameters.

Compound	Substituen	J (cm^{-1})	zJ' (cm^{-1})	Note
5a	H	46.0	-0.25	a
5b	*m*-Ph	47.4	-0.005	a
5c	*m*-CH_3O	35.9	-0.07	a
5d	NO_2	31.0	-0.07	b
5e	$N(CH_3)_2$	34.9	-0.11	b
5f	*t*-Bu	59.3	-0.11	b

Notes: [a]This work. [b]See Ref 1.

III.5 X-Ray Crystallography

The structures of complexes **5a**-**c** were verified by x-ray crystallography. The crystal structures shown in Figure III.4 and the crystallographic parameters are provided in Table III.3. Complete crystallographic files may be found in the supplemental material.

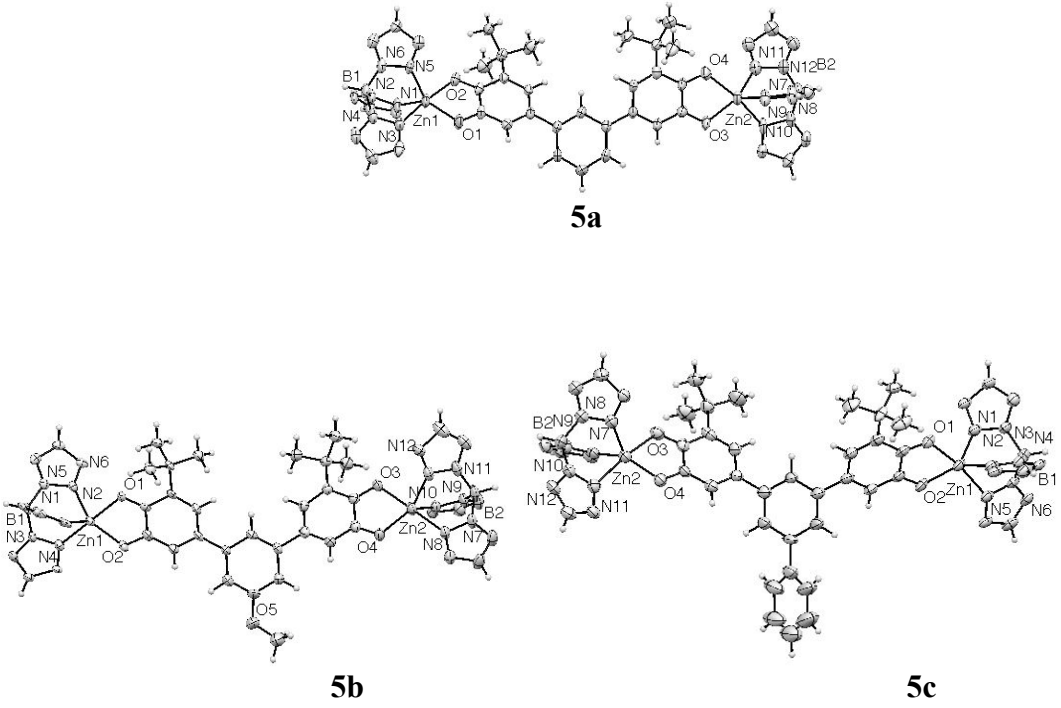

Figure III.4 Bis(Zn^{II}(SQ)$Tp^{Cum,Me}$) Complex ORTEP Drawings.
(Ellipsoids are at the 50% probability level and selected atoms were omitted for clarity.)

Table III.3 Bis(Zn^{II}(SQ)$Tp^{Cum,Me}$) Complex Crystallography Parameters.

Compound	5a	5b	5c
Empirical formula	$C_{104}H_{116}B_2N_{12}O_4Zn_2$	$C_{110}H_{120}B_2N_{12}O_4Zn_2$	$C_{105}H_{118}B_2N_{12}O_5Zn_2$
Formula weight	1750.58	1826.67	1780.35
Temperature (K)	123(2)	108(2)	110
Wavelength	0.71073 A	0.71073	0.71070
Crystal sys, space group	Monoclinic, P2(1)/c	Triclinic, P-1	Triclinic, P1
Unit cell (Å)	a = 11.1192(12) Å α = 90°; b = 21.822(2) Å β = 94.885° (7); c = 44.040(5) Å γ = 90°	a = 11.6009(10) Å α = 76.390°(5); b = 18.5966(16)Å β = 85.934°(6); c = 29.423(3) Å γ = 89.359°(6).	a = 12.3136(5)Å α = 98.021°(3); b = 13.0048(6)Å β = 95.060°(3); c = 33.3571(15)Å γ = 97.950°(2).
Volume (A^3)	10647(2)	6154(9)	5207(4)
Z, Calc density (Mg/m^3)	4, 1.146	2, 1.057	2, 1.137
F(000)	3908	2086	1888
Crystal size (mm)	0.34 x 0.24 x 0.12	0.34 x 0.18 x 0.16	0.28 × 0.20 × 0.06
θ range for data coll	1.84° to 22.10°	1.85° to 22.16°	4.34° to 44.12°
Refls collected/unique	127468/13121	80150/15210	18080/18080
Completeness to θ	99.3 %	98.5 %	99.3 %
Abs corr	Semi-emp from equiv	Semi-emp from equiv	Semi-emp from equiv
Refinement method	Full-matrix least-squares on F^2	Full-matrix least-squares on F^2	Full-matrix least-squares on F^2
Data/restraints/param	13121 / 0 / 1121	15210 / 45 / 1196	18080 / 0 / 1160
Final R indices [I>2sigma(I)]	R1=0.0858, wR2=0.1777	R1 = 0.0605, wR2 = 0.1545	R1=0.0614, wR2=0.1612
GOF	1.092	0.993	1.064
R indices (all data)	R1=0.1057, wR2=0.1865	R1 = 0.1021, wR2 = 0.1704	R1=0.0976, wR2=0.1726
Largest diff. peak & hole	0.970 and -0.700 $e.A^{-3}$	0.491 and -0.365 $e.A^{-3}$	0.656 and -0.556 $e.A^{-3}$
m-phenylene torsion ∠s (°)	38.3, 27.2	37.6, 41.9	33.3, 30.8

III.6 Substituent Effects Study

Spectroscopic, magnetometric and crystallographic properties of these complexes may permit elucidation of substituent effects. These new compounds allow expansion of our investigation of substituent effects on exchange coupling between SQ moieties,[65] to include substituted-SQ-paramagnetic metal ion exchange coupled species.

The shifts in the n $\rightarrow\pi^*$ transitions in the electronic absorption spectra may be linearly related to σ valuesVariation in the ZFS values for D and E measured by EPR can also provide information on changes in spin density distribution. Changes in ***J*** values obtained through SQUID magnetometry as a function of substituent *may* also correlate to Hammett parameters. Finally, examination of the SQ ring torsion angles within this series of complexes may yield information on substituent effects.

To ascertain whether the change in the $n\rightarrow\pi^*$ transition correlates with σ_x for bis(Zn^{II}(SQ)$Tp^{Cum,Me}$) complexes **5a-5c**, we calculated $\Delta\nu_{n\rightarrow\pi^*}$ for the complexes (Table 4).

Table III.4 UV-Vis Absorptions for Bis(Zn^{II}(SQ)$Tp^{Cum,Me}$) Complexes.

	$n\rightarrow\pi^*$ (cm^{-1})	$\Delta\nu_{n\rightarrow\pi^*}$ (cm^{-1})
5a	13,086	0
5b	13,080	-6
5c	14,060	974

Correlations with a number of different σ_x parameters with $\Delta\nu_{n\rightarrow\pi^*}$ values for the Bis(Zn^{II}(SQ)$Tp^{Cum,Me}$) complexes work were explored. Neither σ_{aH}, $\sigma^{\cdot}$, σ^{-}, σ_{para}, σ_{meta} nor the dual parameter $\sigma_{JJ} + \sigma_x$ system provided satisfactory correlations. This leads us to conclude that the substituent influence may be more than a simple inductive effect.

Zero Field Splitting parameters, D/*hc*, related to the distance between the unpaired electrons, and E/*hc*, the magnitude of which depends on the species geometry, were estimated from the simulated spectra and are recorded in Table III.5.

Table III.5 ZFS Parameters for Bis(Zn^{II}(SQ)$Tp^{Cum,Me}$) Complexes.

	D/*hc* (cm^{-1})	E/*hc* (cm^{-1})
5a	0.00399	0.000017
5b	0.00372	0.000042
5c	0.00398	0.000076

Values for the ZFS parameter D obtained for compounds **5a-c** are consistent with values for analogous compounds,[61] and do not vary significantly in magnitude within this series. Thus, we can discern no substituent effect from this data.

A general trend consistent with earlier findings by Bodnar[61] is evident in the data presented in Table 2. Because the magnitude of the exchange parameter ***J*** is related to the magnitude of the exchange integral. The data, taken as a whole, clearly show a two-fold change in ***J***, as a function of substituent. We then used the method of Lahti[13] to determine whether a relationship exists between the spin density, ρ, and ***J*** for our series of radicals by the equation below:

$$\boldsymbol{J}_{calc} = \boldsymbol{J}_0 \rho^A \rho^B \qquad \textbf{Eq. 2}$$

Estimation of the exchange parameter, ***J*** for the bis(semiquinone)s depicted in Figure 5 by Equation 2 gives us a basis for comparison of our experimentally determined ***J***-values. In Table 6, we record the results of spin density calculations at selected carbon centers for our bis(semiquinone)s series.

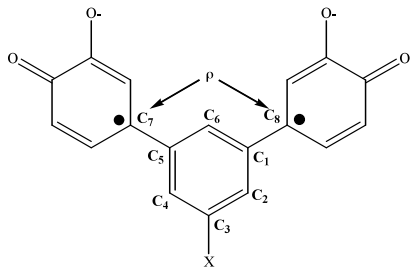

Figure III.5. Substituted Bis(semiquinone) Series showing location of spin densities, ρ_{CX}.

Table III.6. Spin Density Calculations and J_{exp} for Substituted Bis(semiquinone) Series.

Compound	X	J_{exp} (cm^{-1})	$\rho_{[C7,C8]}$ (gauss)	$\Sigma\rho_{[C1-6]}$ (gauss)
5a	H	46.0	0.143, 0.143	0.749
5b	*m*-Ph	47.4	0.101, 0.101	0.851
5c	*m*-CH_3O	35.9	0.132, 0.132	0.789

The theoretical ***J***-value for an unsubstituted bis(semiquinone) with a meta-phenylene linker group, our model compound, was 40-60 cm^{-1}, given a spin density at C_7 and C_8 of 0.18. As Table III.6 shows, J_{exp} was within the range of the theoretical ***J***-value given earlier, except in the cases of complex **5c**. These variations will be addressed momentarily.

As the data shows, calculated values for $\rho_{[C7,C8]}$ were smaller than the spin density for our model compound, and therefore, if Eq. 3 holds, one would anticipate that the exchange coupling parameters would be smaller. All J_{exp} values are below the mid-point of the ***J***–value range for the model compound. The spin densities at C_7 and C_8 for our bis(semiquinone)s are diminished relative to the model compound, with a majority of the spin density being retained in phenyl linker group. In all cases, over one quarter of the available spin density resides in this ring. Unfortunately, neither sets of spin densities correlated to our J_{exp} values.

In order to determine empirically the nature of a substituent effect in the bis(Zn^{II}(SQ)$Tp^{Cum,Me}$) complexes proposed earlier, we investigated the relationship between the exchange parameter, ***J***, and various σ constants. Correlations between ***J***, Δ***J***, log (***J***/$\boldsymbol{J_0}$), and a variety of Hammett sigma values including σ_I, σ_m, $\sigma\cdot$, σ_p, σ^+, and σ_{av} were examined without success. Given this fact, it is difficult to deduce any empirical relationship between ***J*** and established σ systems.

Earlier work has shown that ***J*** can be modulated by torsion angle To determine whether this was the case for bis(Zn^{II}(SQ)$Tp^{Cum,Me}$) complexes, we investigated the possible correlation between ***J*** and the *m*-phenylene torsion angles ϕ_1 and ϕ_2 determined by X-ray crystallography. See Figure III.6 and Table III.7.

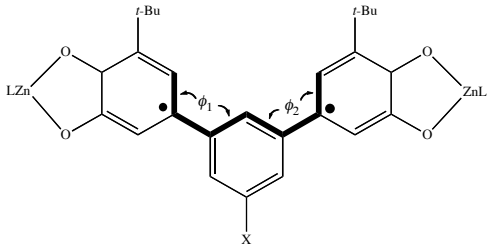

Figure III.6 *m*-phenylene torsion angles ϕ_1 and ϕ_2.

Table III.7 Torsion angles ϕ_1 and ϕ_2 for substituted bis(semiquinone) series.

Compound	X	ϕ_1 (°)	ϕ_2 (°)
5a	H	38.3	27.2
5b	*m*-Ph	37.6	41.9
5c	*m*-CH_3O	33.3	30.8
5d	*m*-NO_2	33.3	33.5
5e	*m*-$N(CH_3)_2$	36.0	31.0
5f	*m*-*t*-Bu	30.2	30.8

Correlations between $(\cos\phi_1)^2(\cos\phi_2)^2$ and ***J*** were examined, but were found to be unsatisfactory ($R < 0.8$). With the exception of **5b**, $\phi_{avg} = 32° \pm 2$, a small variation within the series. Given these facts, it is difficult to assess any definitive modulation of ***J*** by complex conformation in this series. Because of the apparent lack any simple empirical relationship between ***J*** and $\Delta\nu$, a_H, ρ (spin density), known σ parameters or conformational variations, we propose a new set of σ values based on the experimental ***J*** values, using the equation $\log(\boldsymbol{J}_X/\boldsymbol{J}_H) = \rho\sigma_J$. See Table III.8.

Table III.8 σ_J values for substituted bis(semiquinone) series.

Compound	X	σ_J
5a	H	0
5b	*m*-Ph	0.013
5c	*m*-CH_3O	-0.11
5d	*m*-NO_2	-0.17
5e	*m*-$N(CH_3)_2$	-0.12
5f	*m*-*t*-Bu	0.11

While this σ_J scale is tailored to bis(semiquinone) systems, it will be of interest to see if this scale has wider application to other radical complexes.

The results from our study are, however, consistent with and can be explained by previous work.[1] Following is a proposed mechanism of how substituents modulate exchange coupling in bis(Zn^{II}(SQ)$Tp^{Cum,Me}$) complexes.

III.7 Proposed Mechanism of Substituent Modulation of Exchange Coupling.

The magnetic studies show that neither strong electron withdrawing groups nor electron donors facilitate delocalization of the semiquinone radical anions (and therefore, spin density) into the central coupling *m*-phenylene ring so as to increase the ferromagnetic exchange. Nevetheless, these results may be explained using simple Hückel MO theory. [69]

An accurate calculation of the exchange coupling parameter using MO theory must include configuration interaction.[4] This consists of the antiferromagnetic component of the exchange coupling that arises from interaction with low-lying excited states. However, MO theory alone can give a reasonable qualitative description of the magnitude of the ferromagnetic contribution to the overall exchange parameter.[9,65,11]

Hückel MO theory coupled with simple perturbation theory can give a reasonable explanation for the substituent effect on the exchange coupling seen in this work. If we consider the attachment of the a_2 and b_2 symmetry-adapted linear combinations (SALCs) for the CH_2 radical fragments (Figure 7; right) and how they interact with the $1a_2/2a_2$ and $2b_2/3b_2$ frontier MOs of benzene (Figure 7; left) (formally e_{1g} and e_{2u} for D_{6h} symmetry), *meta*-Xylylene SOMOs (Figure 7; middle) can be constructed.

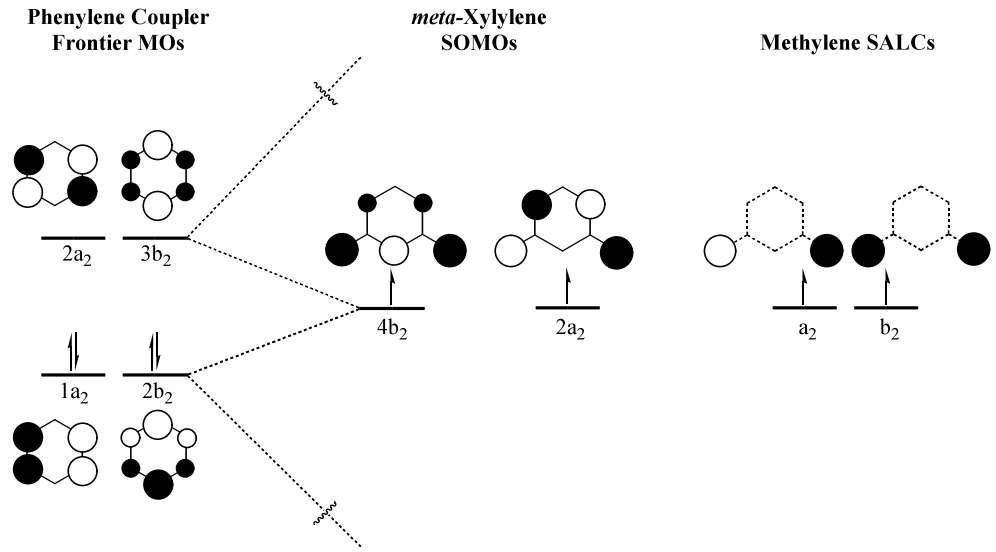

Figure III.7 Construction of *meta*-Xylylene SOMOs using group theory as a guide.

The pairing theorem,[67] stipulates that each set of interactions between the methylene SALCs and the frontier MOs of benzene are equal in magnitude, resulting in two accidentally degenerate SOMOs, $4b_2$ and $2a_2$.

If a mesomeric substituent is attached to the benzene ring, the $2b_2/3b_2$ MOs will mix with the substituent AO, but the $1a_2/2a_2$ will not interact with the substituent AO because the attachment is at nodal positions in these MOs (Figure 7; left). If the newly formed benzyl coupler frontier MOs (Figure 7; left) are interacted with the a_2 and b_2 SALCs of the CH_2 radical fragments, the interaction of the a_2 CH_2-SALC will be identical to that in *meta*-Xylylene, but the interaction of the b_2 CH_2-SALC will be attenuated because of the larger energy gap between the b_2 CH_2-SALC and the benzyl $2b_2$ and $4b_2$ MOs.

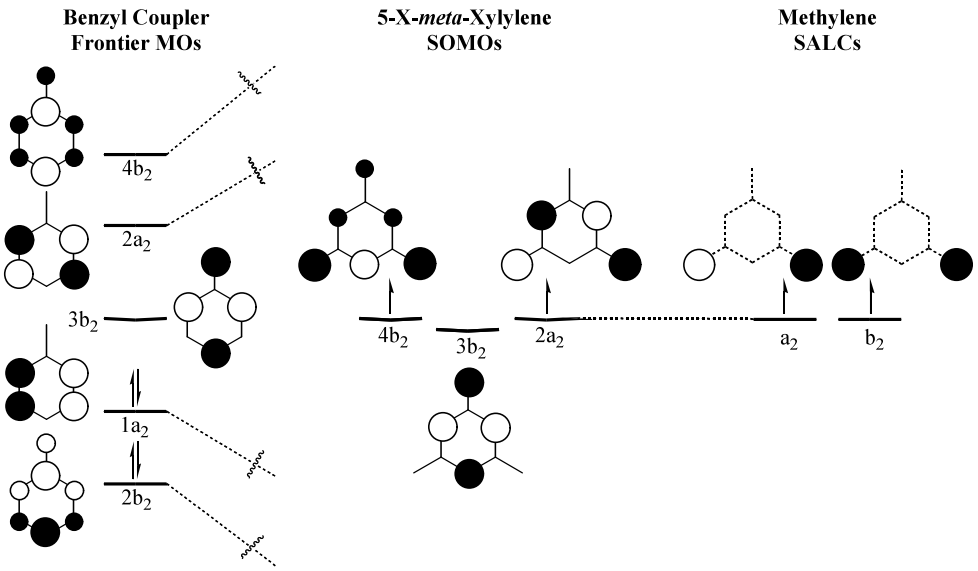

Figure III.8. Construction of 5-X-*meta*-Xylylene SOMOs using group theory as a guide.

This weaker interaction leads to smaller coefficients in the $4b_2$ SOMO and therefore less overlap density between the two 5-X-*meta*-Xylylene SOMOs compared to that of the original *meta*-phenylene.[70] The attenuated overlap density of coefficients of the 5-X-*meta*-Xylylene SOMOs can also be thought of as more disjoint in nature relative to the unsubstituted *meta*-phenylene SOMOs. In other words, attachment of the substituent results in spin density dilution which attenuates the exchange coupling. The OMe, NMe_2 and NO_2 substituents have atoms (oxygen, nitrogen) that are part of the π-system resulting in spin density being delocalized over a larger number of atoms and effectively attenuating the coefficients at other atoms. This can be seen in Figure 8 in the SOMO $4b_2$, where the coefficient on the substituent atom was non-zero. In the *t*-Bu substituent, the quaternary carbon was sp^3-hybridized and was not part of the π-system. The spin-density dilution into this substituent was significantly smaller than the others, and as would be expected the exchange coupling was stronger in the *t*-Bu bis(semiquinone) complex. The other key aspect was that it makes

no difference whether the $3b_2$ 5-X-*meta*-Xylylene orbital was filled or unfilled; both electron pair withdrawers and electron pair donors are predicted to attenuate the exchange integral. This prediction is supported by the magnetic data discussed here and by Borden and Squires' previous work with 1,3,5-trimethylene benzene monoanion. The singlet-triplet gap in this species was calculated to be approximately 50% of the prototype *meta*-xylylene.[69] Their explanation included less overlap of spin-density between SOMOs (more disjoint) as a significant factor in the attenuation of the exchange coupling.

III.8 Conclusion.

The results of the substituent study of the bis(Zn^{II}(SQ)$Tp^{Cum,Me}$) complexes indicate that there may be no straightforward empirical relationship between ***J*** and $\Delta\nu$, spin density, σ, or *m*-phenylene torsion. Therefore, the creation of σ_J values for this series was warranted. Furthermore, the explanation posited by Shultz and Bodnar[61] rationalizing that both electron pair withdrawing and donating substituents attenuate the ***J*** parameter for these complexes, was consistent with the complexes studied here.

References

(1) Petta, J. R.; Slater, S. K.; Ralph, D. C. *Phys. Rev. Lett.* **2004**, *93*, 136601.

(2) Kahn, O. *Molecular Magnetism*; VCH Publishers, Inc: New York, 1993.

(3) Tyndall, J. *Faraday as a Discoverer*; D. Appleton and Company, 1874

(4) Callister, W. D. *Material Science and Engineering an Introduction*; 6th ed.; John Wiley & Sons: New York, 2003

(5) Schwartz, D. A.; Norberg, N. S.; Nguyen, Q. P.; Parker, J. M.; Gamelin, D. R. *J. Am. Chem. Soc.* **2003**, *125*, 13205-13218

(6) Zutic, I.; Fabian, J.; Das Sarma, S. *Rev. of Mod. Phys.* **2004**, *76*, 323.

(7) Madou, M.; Florkey, J. *Chem. Rev.* **2000**, *100*, 2679-2692.

(8) Metzger, R. M. *Chem. Rev.* **2003**, *103*, 3803-3834.

(9) Deng, W.-Q.; Matsuda, Y.; Goddard, W. A. *J. Am. Chem. Soc.* **2007**, *129*, 9834-9835.

(10) Gutlich, P.; Garcia, Y.; Goodwin, H. A. *Chem. Soc. Rev* **2000**, *29*, 419-427.

(11) Reed, M. A.; Chen, J.; Rawlett, A. M.; Price, D. W.; Tour, J. M. *Applied Physics Letters* **2001**, *78*, 3735-3737.

(12) Yoon, D. H.; Lee, S. B.; Yoo, K. H.; Kim, J.; Lim, J. K.; Aratani, N.; Tsuda, A.; Osuka, A.; Kim, D. *Journal of the American Chemical Society* **2003**, *125*, 11062-11064.

(13) Dougherty, E. V. A. a. D. A. *Modern Physical Organic Chemistry*; University Science Books, 2006.

(14) Kahn, O.; VCH Publishers, INC: New York, 1993, p 3.

(15) Shultz, D. A.; Fico, R. M.; Bodnar, S. H.; Kumar, R. K.; Vostrikova, K. E.; Kampf, J. W.; Boyle, P. D. *J. Am. Chem. Soc.* **2003**, *125*, 11761-11771.

(16) Shultz, D. A.; Vostrikova, K. E.; Bodnar, S. H.; Koo, H.-J.; Whangbo, M.-H.; Kirk, M. L.; Depperman, E. C.; Kampf, J. W. *J. Am. Chem. Soc.* **2003**, *125*, 1607-1617.

(17) Shultz, D. A.; Bodnar, S. H.; Vostrikova, K. E.; Kampf, J. W. *Inorg. Chem.* **2000**, *39*, 6091-6093.

(18) Kramers, H. A. *Physica* **1934**, *1*, 182-192.

(19) Lahti, P. M.; Ichimura, A. S.; Sanborn, J. A. *J. Phys. Chem. A* **2000**, *105*, 251-260.

(20) Miller, S. L. A.; Marsh, E.; Bushard, P.; Wasielewski, M. R. *J. Am. Chem. Soc.* **2000**, *122*, 7802-7810.

(21) Rajca, A. *Chem. Rev.* **1994**, *94*, 871-893.

(22) McConnell, H. M. *J. Chem. Phys.* **1961**, *35*, 508-515.

(23) Li, S.; Ma, J.; Jiang, Y. *J. Phys. Chem.* **1996**, *100*, 4775-4780.

(24) Longuet-Higgins, H. C. *J. Chem. Phys.* **1950**, *18*, 265-274.

(25) Longuet-Higgins, H. C. *J. Chem. Phys.* **1950**, *18*, 275-282.

(26) Longuet-Higgins, H. C. *J. Chem. Phys.* **1950**, *18*, 283-281.

(27) Zilberg, S.; Haas, Y. *J. Phys. Chem. A* **1998**, *102*, 10851-10859.

(28) Shultz, D.A., Bodnar, S. H., Lee, H., Kampf, J. W., Incarvito, C.D., Rheingold, A.L. *J. Amer. Chem. Soc.* **2002**, *124*, 10054.

(29) Shultz, D. A., Bodnar, S. H.; Vostrikova, K. E.; Koo, H-J., Whangbo, M-H., Kirk, M., Depperman, E., Kampf, J. W. *J. Chem. Soc.* **2003**, *125*, 1607.

(30) Brüker WINEPR Simfonia, 1.25, Shareware version; Brüker Analytische Messtechnik GmbH: Rheinstetten, Germany, **1996**.

(31) Kahn, O. *Molecular Magnetism*; VCH Publishers, Inc.: New York, **1993**.

(32) Bleaney, B. B., K. D. *Proc. R. Soc. London.* **1952**, *A214*, 451.

(33) Martin L. Kirk, David A. Shultz, Diana Habel-Rodriguez, Robert D. Schmidt and Ubie Sullivan ***J. Phys. Chem. B*** 2010, ***114,*** **14712–14716**

(34) O'Connor, C. J. *Prog. Inorg. Chem.* **1982**, *29*, 203.

(35) Caneschi, A. D., A.; Mussari, C.P.; Shultz, D.A.; Sorace, L.; Vostrikova, K.E. *Inorg. Chem.* **2002**, *41*, 1086.

(36) Borden, W. T., Squires, R.R., Kemnitz, C.R. *J. Am. Chem. Soc.* **1997**, *119*, 6564.

(37) Borden, W. T.; Iwamura, H.; Berson, J. A. *Acc. Chem. Res.* **1994**, *27*, 109.

(38) Davidson, E. R., Borden, W. T. *J. Am. Chem. Soc.* **1977**, *99*, 4587.

(39) Borden, W. T., Davidson, E. R. *Acc. Chem. Res.* **1981**, *14*, 69.

(40) Lahti, P. ed. *Magnetic Properties of Organic Materials*. Marcel Dekker, Inc.: New York. **1999**, p. 253.

(41) Salem, L. *Molecular Orbital Theory of Conjugated Systems*; W.A. Benjamin Inc.: New York, **1966**.

(42) Rajca, A. *Chem. Rev.* **1994**, *94*, 871.
(43) Dougherty, D. A. *Acc. Chem. Res.* **1991**, *24*, 88.

(44) Shultz, D. A., Boal, A. K.**,** Driscoll, D.J., Farmer, G.T., Kitchin, J.R., Miller, D.B., Tew, G.N. *Mol. Cryst. Liq. Cryst***. 1997,** Vol 305, 303.

(45) Kelly, T., Bridger, G., Zhao, C. *J. Amer. Chem. Soc.* **1990**, *112*, 8024.

(46) Dorman, L. *J. Org. Chem.* **1966**, *31*, 3666.

(47) Davis, W. B.; Ratner, M. A.; Wasielewski, M. R. *Chem. Phys.* **2002**, *281*, 333–346.

(48) Kirk, M. L.; Shultz, D. A.; Depperman, E. C.; Brannen, C. L. *J. Am. Chem. Soc.* **2007**, *129*, 1937–1943.

(49) Weiss, E. A.; Ahrens, M. J.; Sinks, L. E.; Gusev, A. V.; Ratner, M. A.; Wasielewski, M. R. *J. Am. Chem. Soc.* **2004**, *126*, 5577.

(50) Weiss, E. A.; Ahrens, M. J.; Sinks, L. E.; Ratner, M. A.; Wasielewski, M. R. *J. Am. Chem. Soc.* **2004**, *126*, 9510.

(51) Weiss, E. A.; Tauber, M. J.; Kelley, R. F.; Ahrens, M. J.; Ratner, M. A.; Wasielewski, M. R. *J. Am. Chem. Soc.* **2005**, *127*, 11842.

(52) Weiss, E. A.; Wasielewski, M. R.; Ratner, M. A. *J. Chem. Phys.* **2005**, *123*, 064504.

(53) Depperman, E. C.; Bodnar, S. H.; Vostrikova, K. E.; Shultz, D. A.; Kirk, M. L. *J. Am. Chem. Soc.* **2001**, *123*, 3133.

(54) Kirk, M. L.; Shultz, D. A.; Depperman, E. C. *Polyhedron* **2005**, *24*, 2880–2884.

(55) Weiss, E. A.; Ratner, M. A.; Wasielewski, M. R. *J. Phys. Chem. A* **2003**, *107*, 3639–3647.

(56) Weiss, E. A.; Tauber, M. J.; Ratner, M. A.; Wasielewski, M. R. *J. Am. Chem. Soc.* **2005**, *127*, 6052.

(57) Kirk, M. L.; Shultz, D. A.; Schmidt, R. D.; Habel-Rodriguez, D.; Lee, H.; Lee, J. *J. Am. Chem. Soc.* **2009**, *131*, 18304–18313.

(58) Shultz, D. A.; Vostrikova, K. E.; Bodnar, S. H.; Koo, H. J.; Whangbo, M. H.; Kirk, M. L.; Depperman, E. C.; Kampf, J. W. *J. Am. Chem. Soc.* **2003**, *125*, 1607.

(59) Stoll, S.; Schweiger, A. *J. Magn. Reson.* **2006**, *178*, 42–55.

(60) Sloop, J. C., Shultz, D. A., Coote, T., Shepler, B., Sullivan, U., Kampf, J. W. and Boyle, P. D. (2012), J. Phys. Org. Chem., 25: 314–321. doi: 10.1002/poc.1917

(61) D. A. Shultz, S. H Bodnar, H. Lee, J. W. Kampf, C. D. Incarvito, A. L. Rheingold, J. Am. Chem. Soc. 2002a, 124, 10054.

(62) D.A. Shultz, S. H Bodnar, K. E. Vostrikova, H-J. Koo, M.-H. Whangbo, M. Kirk, E. Depperman, J. W. Kampf, J. Chem. Soc.. 2003a, 125, 1607.

(63) Bruker WINEPR Simfonia, 1.25, Shareware Version, Bruker Analy-tische Messtechnik GmbH, Rheinstetten, Germany, 1996

(64) C. J. O'Connor, Prog. Inorg. Chem. 1982, 29, 203.

(65) W. T. Borden, H. Iwamura, J. A. Berson, Acc. Chem. Res. 1994, 27, 109.

(66) W. T. Borden, E. R. Davidson, Acc. Chem. Res. 1981, 14, 69.

(67) C. K. Hancock, D. Clague, J. Am. Chem. Soc. 1964, 86, 4942.

(68) P. J. Sephens, F. J. Devlin, C. F. Chabalowski, M. J. Frisch, J. Phys. Chem. 1994, 98, 11623.

(69) W. T. Borden, R. R. Squires, C. R. Kemnitz, J. Am. Chem. Soc. 1997, 119, 6564.

(70) J. E. Wertz, J. R. Bolton, Electron Spin Resonance, Chapman and Hall, 1986.

Appendix

Zeroth Order Energies of States

The Energy of the closed shell singlet is:

$$E_{CS,S} = 1/2\left\langle A(1)\,A(2) - B(1)\,B(2)\right| h(1)+h(2)\left| A(1)\,A(2) - B(1)\,B(2)\right\rangle$$
$$= .5[\left\langle A(1)\,A(2)\right| h(1)+h(2)\left| A(1)\,A(2)\right\rangle - \left\langle A(1)\,A(2)\right|h(1)+h(2)\left| B(1)\,B(2)\right\rangle$$
$$- \left\langle B(1)\,B(2)\ \right| h(1)+h(2)\left|A(1)\,A(2)\right\rangle + \left\langle B(1)\,B(2)\right|h(1)+h(2)\left|B(1)\,B(2)\right\rangle]$$
$$= .5\left[\left\langle A(2)\right|A(2)\right\rangle\left\langle A(1)\right|h(1)\left|A(1)\right\rangle + \left\langle A(1)\right|A(1)\left\rangle\right\langle A(2)\left|h(2)\right|A(2)\right\rangle$$
$$-\left\langle A(2)\right|B(2)\left\rangle\right\langle A(1)\left|h(1)\right|B(1)\right\rangle - \left\langle A(1)\right|B(1)\left\rangle\right\langle A(2)\left|h(2)\right|B(2)\right\rangle$$
$$-\left\langle B(2)\right|A(2)\left\rangle\right\langle B(1)\left|h(1)\right|A(1)\right\rangle - \left\langle B(1)\right|A(1)\left\rangle\right\langle B(2)\left|h(2)\right|A(2)\right\rangle$$
$$+\left\langle B(2)\right|B(2)\left\rangle\right\langle B(1)\left|h(1)\right|B(1)\right\rangle + \left\langle B(1)\right|B(1)\left\rangle\right\langle B(2)\left|h(2)\right|B(2)\right\rangle]$$

The above math simplifies to:

$$\frac{1}{2}(\alpha+\alpha-0-0-0-0+\alpha+\alpha) = 2\alpha$$

The energy of the other closed shell singlet is:

$$E_{CS,S} = 1/2\left\langle A(1)\,A(2) + B(1)\,B(2)\right| h(1)+h(2)\left| A(1)\,A(2) + B(1)\,B(2)\right\rangle$$
$$= .5[\left\langle A(1)\,A(2)\right| h(1)+h(2)\left| A(1)\,A(2)\right\rangle + \left\langle A(1)\,A(2)\right|h(1)+h(2)\left| B(1)\,B(2)\right\rangle$$
$$+ \left\langle B(1)\,B(2)\ \right| h(1)+h(2)\left|A(1)\,A(2)\right\rangle + \left\langle B(1)\,B(2)\right|h(1)+h(2)\left|B(1)\,B(2)\right\rangle]$$
$$= .5\left[\left\langle A(2)\right|A(2)\right\rangle\left\langle A(1)\right|h(1)\left|A(1)\right\rangle + \left\langle A(1)\right|A(1)\left\rangle\right\langle A(2)\left|h(2)\right|A(2)\right\rangle$$
$$+\left\langle A(2)\right|B(2)\left\rangle\right\langle A(1)\left|h(1)\right|B(1)\right\rangle + \left\langle A(1)\right|B(1)\left\rangle\right\langle A(2)\left|h(2)\right|B(2)\right\rangle$$
$$+\left\langle B(2)\right|A(2)\left\rangle\right\langle B(1)\left|h(1)\right|A(1)\right\rangle + \left\langle B(1)\right|A(1)\left\rangle\right\langle B(2)\left|h(2)\right|A(2)\right\rangle$$
$$+\left\langle B(2)\right|B(2)\left\rangle\right\langle B(1)\left|h(1)\right|B(1)\right\rangle + \left\langle B(1)\right|B(1)\left\rangle\right\langle B(2)\left|h(2)\right|B(2)\right\rangle]$$

This simplifies to:

$$\frac{1}{2}(\alpha+\alpha+0+0+0+0+\alpha+\alpha) = 2\alpha$$

The energy of the open shell single is:

$$E_{OS,S} = 1/2\left\langle A(1)\,B(2) + B(1)\,A(2)\right|\,h(1)+h(2)\,\left|A(1)\,B(2) + B(1)\,A(2)\right\rangle$$
$$= .5[\left\langle A(1)\,B(2)\right|\,h(1)+h(2)\,\left|A(1)\,B(2)\right\rangle + \left\langle A(1)\,B(2)\right|h(1)+h(2)\,\left|B(1)\,A(2)\right\rangle$$
$$+\left\langle B(1)\,A(2)\,\right|\,h(1)+h(2)\left|A(1)\,B(2)\right\rangle + \left\langle B(1)\,A(2)\right|h(1)+h(2)\left|B(1)\,A(2)\right\rangle]$$
$$= .5\,[\left\langle B(2)\middle|B(2)\right\rangle\left\langle A(1)\middle|h(1)\middle|A(1)\right\rangle + \left\langle A(1)\middle|A(1)\right\rangle\left\langle B(2)\middle|h(2)\middle|B(2)\right\rangle$$
$$+\left\langle A(2)\middle|B(2)\right\rangle\left\langle A(1)\middle|h(1)\middle|B(1)\right\rangle + \left\langle A(1)\middle|B(1)\right\rangle\left\langle A(2)\middle|h(2)\middle|B(2)\right\rangle$$
$$+\left\langle B(2)\middle|A(2)\right\rangle\left\langle B(1)\middle|h(1)\middle|A(1)\right\rangle + \left\langle B(1)\middle|A(1)\right\rangle\left\langle B(2)\middle|h(2)\middle|A(2)\right\rangle$$
$$+\left\langle A(2)\middle|A(2)\right\rangle\left\langle B(1)\middle|h(1)\middle|B(1)\right\rangle + \left\langle B(1)\middle|B(1)\right\rangle\left\langle A(2)\middle|h(2)\middle|A(2)\right\rangle]$$

This simplifies to:

$$\frac{1}{2}(\alpha+\alpha+0+0+0+0+\alpha+\alpha) = 2\alpha$$

The Energy of the Triplet is:

$$E_{Triplet} = 1/2\left\langle A(1)\,B(2) - B(1)\,A(2)\right|\,h(1)+h(2)\,\left|A(1)\,B(2) - B(1)\,A(2)\right\rangle$$
$$= .5[\left\langle A(1)\,B(2)\right|\,h(1)+h(2)\,\left|A(1)\,B(2)\right\rangle - \left\langle A(1)\,B(2)\right|h(1)+h(2)\,\left|B(1)\,A(2)\right\rangle$$
$$-\left\langle B(1)\,A(2)\,\right|\,h(1)+h(2)\left|A(1)\,B(2)\right\rangle + \left\langle B(1)\,A(2)\right|h(1)+h(2)\left|B(1)\,A(2)\right\rangle]$$
$$= .5\,[\left\langle B(2)\middle|B(2)\right\rangle\left\langle A(1)\middle|h(1)\middle|A(1)\right\rangle + \left\langle A(1)\middle|A(1)\right\rangle\left\langle B(2)\middle|h(2)\middle|B(2)\right\rangle$$
$$-\left\langle A(2)\middle|B(2)\right\rangle\left\langle A(1)\middle|h(1)\middle|B(1)\right\rangle + \left\langle A(1)\middle|B(1)\right\rangle\left\langle A(2)\middle|h(2)\middle|B(2)\right\rangle$$
$$-\left\langle B(2)\middle|A(2)\right\rangle\left\langle B(1)\middle|h(1)\middle|A(1)\right\rangle + \left\langle B(1)\middle|A(1)\right\rangle\left\langle B(2)\middle|h(2)\middle|A(2)\right\rangle$$
$$+\left\langle A(2)\middle|A(2)\right\rangle\left\langle B(1)\middle|h(1)\middle|B(1)\right\rangle + \left\langle B(1)\middle|B(1)\right\rangle\left\langle A(2)\middle|h(2)\middle|A(2)\right\rangle]$$

This simplifies to:

$$\frac{1}{2}(\alpha+\alpha-0-0-0-0+\alpha+\alpha) = 2\alpha$$

To zeroth order, (i.e., ignoring electron/electron repulsion) all energies are degenerate.

Energies after accounting for e-/e- repulsion

The Energy of the closed shell singlet is:

$$E_{CS,S} = 1/2\left\langle A(1)\,A(2) - B(1)\,B(2)\left|\frac{1}{r_{12}}\right| A(1)\,A(2) - B(1)\,B(2)\right\rangle$$

$$= .5[\left\langle A(1)\,A(2)\left|\frac{1}{r_{12}}\right| A(1)\,A(2)\right\rangle - \left\langle A(1)\,A(2)\left|\frac{1}{r_{12}}\right| B(1)\,B(2)\right\rangle$$

$$- \left\langle B(1)\,B(2)\left|\frac{1}{r_{12}}\right| A(1)\,A(2)\right\rangle + \left\langle B(1)\,B(2)\left|\frac{1}{r_{12}}\right| B(1)\,B(2)\right\rangle]$$

This simplifies to:

$$\frac{1}{2}\left(j^o - k + j^o - k\right) = j^o - k$$

Incorporating the energy from the zeroth order Hamiltonian yields a final energy of:

$$E = 2\alpha + j^o + k$$

The energy of the other closed shell singlet is:

$$E_{CS,S} = 1/2\left\langle A(1)\,A(2) + B(1)\,B(2)\left|\frac{1}{r_{12}}\right| A(1)\,A(2) + B(1)\,B(2)\right\rangle$$

$$= .5\left[\left\langle A(1)\,A(2)\left|\frac{1}{r_{12}}\right| A(1)\,A(2)\right\rangle + \left\langle A(1)\,A(2)\left|\frac{1}{r_{12}}\right| B(1)\,B(2)\right\rangle\right.$$

$$\left. + \left\langle B(1)\,B(2)\left|\frac{1}{r_{12}}\right| A(1)\,A(2)\right\rangle + \left\langle B(1)\,B(2)\left|\frac{1}{r_{12}}\right| B(1)\,B(2)\right\rangle\right]$$

This simplifies to:

$$\frac{1}{2}\left(j^o + k + j^o + k\right) = j^o + k$$

Incorporating the energy from the zeroth order Hamiltonian yields a final energy of:

$$E = 2\alpha + j^o + k$$

The energy of the open shell single is:

$$E_{OS,S} = 1/2\left\langle A(1)\,B(2) + B(1)\,A(2)\left|\frac{1}{r_{12}}\right| A(1)\,B(2) + B(1)\,A(2)\right\rangle$$

$$= .5\left[\left\langle A(1)\,B(2)\left|\frac{1}{r_{12}}\right| A(1)\,B(2)\right\rangle + \left\langle A(1)\,B(2)\left|\frac{1}{r_{12}}\right| B(1)\,A(2)\right\rangle\right.$$

$$\left. + \left\langle B(1)\,A(2)\left|\frac{1}{r_{12}}\right| A(1)\,B(2)\right\rangle + \left\langle B(1)\,A(2)\left|\frac{1}{r_{12}}\right| B(1)\,A(2)\right\rangle\right]$$

This simplifies to:

$$\frac{1}{2}\left(j + k + j + k\right) = j + k$$

Incorporating the energy from the zeroth order Hamiltonian yields a final energy of:

$$E = 2\alpha + j + k$$

The Energy of the Triplet is:

$$E_{Triplet} = 1/2\left\langle A(1)\,B(2) - B(1)\,A(2)\left|\frac{1}{r_{12}}\right| A(1)\,B(2) - B(1)\,A(2)\right\rangle$$

$$= .5\left[\left\langle A(1)\,B(2)\left|\frac{1}{r_{12}}\right| A(1)\,B(2)\right\rangle - \left\langle A(1)\,B(2)\left|\frac{1}{r_{12}}\right| B(1)\,A(2)\right\rangle\right.$$

$$\left. - \left\langle B(1)\,A(2)\left|\frac{1}{r_{12}}\right| A(1)\,B(2)\right\rangle + \left\langle B(1)\,A(2)\left|\frac{1}{r_{12}}\right| B(1)\,A(2)\right\rangle\right]$$

This simplifies to:

$$\frac{1}{2}\left(j - k + j - k\right) = j - k$$

Incorporating the energy from the zeroth order Hamiltonian yields a final energy of:

$$E = 2\alpha + j - k$$

Experimental Section

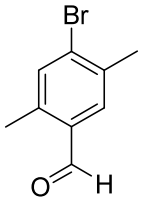

4-Bromo-2,5-dimethylbenzaldehyde (II.7). A 100 mL Schlenk flask containing 1,4-dibromo-2,5-dimethylbenzene (3 g, 11.36 mmol) in 75 mL of distilled THF was cooled to -78°C under a flow of N_2. To the reaction mixture was added two equivalents of t-butyl lithium (15.15 mL) via syringe and stirred for 30 minutes. Distilled DMF (5.00 mL) was added and the Schlenk flask was removed from the cold bath. The reaction was stirred overnight and quenched with 15 mL water. The product was separated by column chromatography using pet ether/ether 90/10 to yield **II.7** as a white solid (1.63 g, 70%). ^{1}H NMR (300MHz, $CDCl_3$) δ (ppm): 10.20 (s, 1H), 7.64 (s, 1H), 7.47 (s, 1H), 2.31 (s, 3H), 2.43 (s, 3H). ^{13}C NMR (300MHz, $CDCl_3$) δ (ppm): 192.1, 139.47, 136.66, 135.65, 133.78, 133.25, 131.53, 22.44, 18.74.

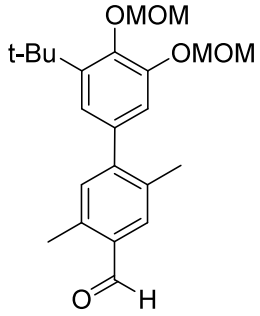

3'-*tert*-Butyl-4',5'-bis-methoxymethoxy-phenyl-2,5-dimethyl-4-carbaldehyde (II.10). A 50 mL Schlenk flask containing **II.7** (.768 g, 3.61 mmol), **3'-*tert*-Butyl-4',5'-bis-methoxymethoxy paraxylene boronic ester** (1.00 g, 3.28 mmol), $Pd(PPh_3)_4$ (.379 g, 10%), Na_2CO_3 (2 M, 4.62 mL) and ethanol (5 mL) in distilled THF (100 mL) was pump/purged under N_2 three times. The reaction mixture was refluxed for 36 hours and the solvent was removed under reduced pressure. The crude material was diluted with ether and filtered through a pad of Celite. The filtrate was then extracted with a separatory funnel using DCM and brine followed by deionized H_2O then dried over Na_2SO_4, filtered, and evaporated to dryness. The brown/yellow oil was purified RPLC (20% ether in petroleum ether) to give **II.10** (5.4 g, 74%) as a white crystalline solid. ^{1}H NMR (300MHz, $CDCl_3$) δ (ppm): 10.27 (s, 1H), 7.68 (s, 1H), 7.12 (s, 1H), 6.83 (d, 1H, J = 1.95 Hz), 6.70 (d, 2H, J = 1.95 Hz), 5.72 (s, 1H), 2.66 (s, 3H), 2.33 (s, 3H), 1.45 (s, 9H)

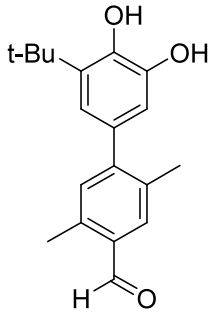

3'-*tert*-Butyl-4',5'-bis-hydroxy-phenyl-2,5-dimethyl-4-carbaldehyde (h). A 50 mL round bottom flask containing **II.10** (.200 g, 5.17 mmol) in methanol was added 3 drops of 12 M HCl and refluxed overnight. The mixture was quenched with 10 mL H_2O and separated using Ether/Water. Ether was removed under reduced pressure to yield **h** (.150 g, 98%) as a colorless solid. ^{1}H NMR (300MHz, $CDCl_3$) δ (ppm): 10.27 (s, 1H), 7.68 (s, 1H), 7.12 (s, 1H), 6.83 (d, 1H, *J* = 1.95 Hz), 6.70 (d, 2H, *J*=1.95 Hz), 5.72 (s, 1H), 2.66 (s, 3H), 2.33 (s, 3H), 1.45 (s, 9H).

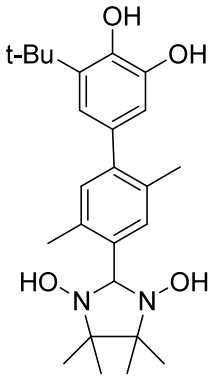

2-(3'-*tert*-Butyl-4',5'-dihydroxy-paraxylene-4-yl)-4,4,5,5-tetramethyl-imidazolidine-1,3-diol (i). A 50 mL round bottom flask containing **h** (160mg, .537mmol) in methanol was added 4,4,5,5-tetramethyl bis-hydroxyl amine (95 mg .641 mmol). The reaction vessel was stirred at room temperature for 36 hours. Solvent was removed under reduced pressure, to yield yellow powder, however no further purification was conducted due to the instability of the product. ^{1}H NMR (300MHz, $CDCl_3$) δ (ppm): 7.52 (s, 1H), 7.03 (s, 1H), 6.82 (d, 1H), 6.48 (d, 1H), 5.21(s, 1H), 2.47 (s, 3H), 2.28 (s, 3H), 1.48 (s, 9H), 1.23 (s, 6H), 1.22 (s, 6H).

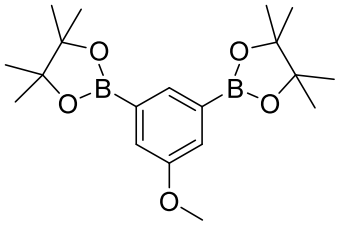

3,5-Bis(4,4,5,5-tetramethyldioxaborane) anisole (II.4). To a 100 mL round bottom flask was added 3,5-dibromo anisole (1.73 g, 6.5 mmol), bis(pinacolato) diboron (3.65 g, 13 mmol) and potassium acetate (4.5 g, 45 mmol) under N_2. $PdCl_2$(dppf) was weighed (790 mg) in the dry box and transferred to the reaction vessel. Reaction mixture was stirred at 70^{o}C for 48hrs. Purification requires two techniques due to similar R_F. Bis(pinacolato)diboron was removed using sublimation at 85^{o}C using tap water to cool apparatus. The resulting brown oil was purified on a chromatotron using 85% ethyl acetate/15% hexanes (1.35 g 60%). ^{1}H NMR (300MHz, $CDCl_3$) δ (ppm): 7.88 (d, 1H, *J*=.73Hz), 7.43 (s, 2H), 3.85 (s, 3H), 3.64 (s, 24H).

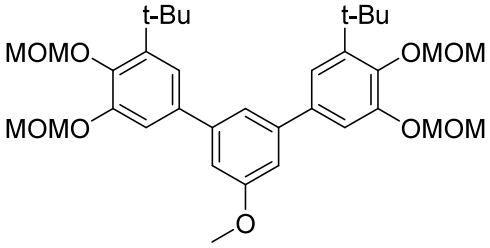

3,5-Bis-(5-*t*-butyl-3,4-methoxymethyl)anisole (II.5). A 100 mL Schlenk flask containing **II.4** (.500 g, 1.45 mmol), MOMBr (.962g, 2.90 mmol), $Pd(PPh_3)_4$ (5 mol%), EtOH (5 mL), and 40 mL of distilled THF was pumped and purged three times under nitrogen atmosphere followed by the addition of 2M Na_2CO_3 (5 mL) via syringe. The reaction mixture was again pumped and purged three times. The reaction mixture was refluxed for 18 hours followed by solvent removal under reduced pressure, ether was added and the reaction mixture was filtered on Celite. The remaining crude mixture was purified by column chromatography with 20:80 (hexanes: ethyl acetate) to give **II.5** (.667 g, 75%) as a light yellow oil. ^{1}H NMR (300MHz, DMSO): 7.29 (s, broad 2H), 7.26 (s, broad 1H), 7.17 (s, 2H), 7.06 (s, broad 2H), 5.29 (s, 4H), 5.19 (s, 4H), 3.87 (s, 3H), 3.57 (s, 6H) 3.44 (s, 6H), 1.42 (s, 18H).

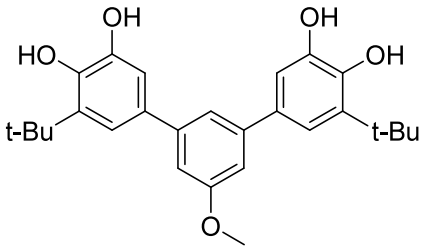

3,5-Bis-(5-*t*-butyl-3,4-hydroxy)anisole. To a 100 mL round bottom flask containing 50 mL of distilled methanol was added **3,5-Bis-(5-*t*-butyl-3,4-methoxymethyl)anisole (II.5**) (200 mg, 0.326 mmol) and 3 drops of concentrated acid (HCl). The reaction was heated to reflux for 12 hr. After cooling, the solution was washed with saturated $NaHCO_3$, then with brine, and finally dried over Na_2SO_4. Solvent was removed by rotary evaporation to yield **3,5-Bis-(5-*t*-butyl-3,4-methoxymethyl)anisole** as a yellow oil (.139 g, 98%). ^{1}H NMR (300MHz, DMSO): 7.22 (m, 1H), 7.14 (d, 2H, *J*=1.95), 7.00 (d, 2H *J*=1.95), 6.98 (d, 2H, *J*=1.46), 5.69 (s, 2H), 4.87 (s, 2H), 3.91 (s, 3H), 1.47 (s, 18H).

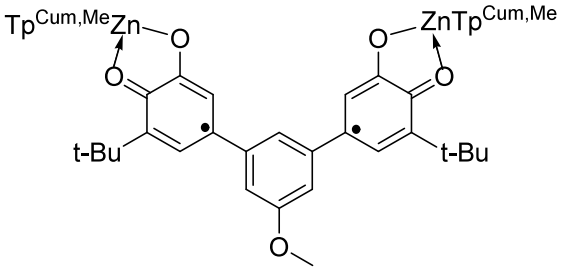

Complexed Methoxy Phenyl Bis(Semiquinone) (II.6). To a 100 mL Schlenk flask containing 30 mL of a 50/50 mixture of distilled methanol and methylene chloride, the bis(catechol) **3,5-Bis-(5-*t*-butyl-3,4-hydroxy)anisole** (.149 g, 0.320 mmol) and $Zn(OH)TP^{Cum, Me}$ (.221 g, .320 mmol). The reaction mixture was stirred under inert atmosphere for one hour. The reaction mixture was then exposed to air, stirred overnight, and finally filtered through filter paper to yield the desired complex as a dark green solid (.195 g, 55%).

Instrumentation. NMR data were collected on a Varian VXR-300 NMR. All ^{1}H and ^{13}C NMR chemical shifts reported are referenced to deuteriochloroform at the appropriate

chemical shift unless specifically noted. IR data were collected using a Perkin-Elmer 1600 FT-IR spectrometer. High resolution mass spectrometric analytical determinations were performed by the North Carolina State University Mass Spectral Facility. Elemental analyses were performed by Atlantic Microlab, Inc. Melting points were obtained on a Mel-temp melting point apparatus and are uncorrected. X-band EPR spectra were recorded on an IBM-Bruker E200SRC spectrometer. Frozen solution EPR spectroscopy was performed on 1mM solutions of the bis(Zn^{II}(SQ)TpCum,Me) complexes in Me-THF. Magnetometry data was collected using a Quantum Design MPMSXL SQUID magnetometer.

Chemicals. 1,3-dibromobenzene was purchased from Aldrich Chemical company and were used without further purification. Compounds **1a** ,[16] **1b**,[16] 3,5-dibromobiphenyl[17] and 3,5-dibromoanisole[18] were prepared according to literature methods. All reactions, solvent distillations and EPR sample preparation were conducted under nitrogen or argon atmosphere. Solvents were purchased from Fisher Scientific or Aldrich, and unless otherwise noted, were freshly distilled immediately prior to use. THF was distilled from sodium benzophenone-ketyl before use, while CH_2Cl_2 and CH_3OH were distilled from CaH_2.

General Procedure for the Synthesis of bis(metaphenylene)s (3).

To a Keldahl flask was added the 1,3-dibromoarene (1 eq), **1a** or **1b** (2 eq), $Pd(PPh_3)_4$ (5-10 mol%), dry THF (25-50mL), EtOH (5-15 mL), 2M Na_2CO_3 (7-22mL), and reaction flask was purged 3 times w/ N_2. To this was added a reflux condenser, the flask covered with aluminum foil and refluxed for 18-36h. The crude product was taken up in CH_2Cl_2 and filtered through Celite. This solution was washed w/ saturated NaCl, dried over Na_2SO_4, and concentrated under reduced pressure. Resulting crude product was recrystallized or

subjected to chromatography (Et_20/CH_2Cl_2/P.E gradient elution), affording the bis(metaphenylene).

General Procedures for the Preparation of Catechols (4):

Method A. To a 100mL round bottom flask equipped with a stir bar was added the *t* -Butyl-bis(methoxymethyl)biphenyl (~ 1-3 mmol), concentrated HCl (2mL), and methanol (50-70mL). A reflux condenser was attached, and the mixture refluxed for 18h with stirring under N_2, protected from light. The solvent was removed by evaporation under reduced pressure. The residue was taken up in CH_2Cl_2, extracted with saturated brine, and the bottom organic layer dried over Na_2SO_4. The solvent was evaporated to dryness to afford the catechol.

Method B. To a 125 mL Keldahl flask equipped with a N_2 adapter and stir bar was added the *t* -Butyl-dimethoxybiphenyl (1 equivalent, ~0.5-1.5mmol), distilled CH_2Cl_2 (~10mL), purged 3X with N_2, and cooled to -78^oC. Then, a 1.0M solution of BBr_3 (3 equivalents, ~1.5-4.5mmol), was added dropwise slowly to the reaction mixture, which was then allowed to warm to room temperature and stir for 20h under N_2, protected from light. The reaction mixture was quenched with ice, washed with saturated brine and extracted with two 10mL portions of CH_2Cl_2. The organic layers were combined, dried over Na_2SO_4, and the solvent evaporated to dryness to afford the catechol.

General Procedure for the Synthesis of Bis(Zn^{II}(SQ)$Tp^{Cum,Me}$) Complexes (5):

To a 100mL round bottom flask was added 1 equivalent $KTp^{Cum,Me}$ (~0.2mmol), 30mL distilled CH_2Cl_2, 1 equivalent $Zn(ClO_4)_2 \cdot 6H_2O$ (~0.2mmol), and 4.5mL N_2 saturated methanol. The mixture was stirred until all reagents dissolved (15-30min). Then, 0.5

equivalents of the bis(catechol) (~0.1mmol) was added to the flask and the reaction mixture stirred under N_2 for an additional 1h. Finally, triethylamine (0.695mL of a 4% solution v:v with CH_2Cl_2) was delivered via syringe into the reaction flask and the mixture stirred for an additional 1.5h. The reaction flask was opened to air and stirred overnight. The greenish-brown solution was concentrated under reduced pressure. The resulting solid was washed with diethyl ether, filtered, and the solvent removed under reduced pressure. The resulting microcrystalline product was recrystallized, affording the complex.